NOVA SCHOOL OF SCIENCE & TECHNOLOGY

DEPARTMENT OF PHYSICS

MARTA ISABEL RAMOS MARQUES

BSc in Biomedical Engineering

ELECTRO-RESPONSIVE ON-DEMAND DRUG DELIVERY SYSTEM FOR E-PATCHES

MASTER IN BIOMEDICAL ENGINEERING

NOVA University Lisbon

April, 2024

NOVA SCHOOL OF SCIENCE & TECHNOLOGY

DEPARTMENT OF PHYSICS

ELECTRO-RESPONSIVE ON-DEMAND DRUG DELIVERY SYSTEM FOR E-PATCHES

MARTA ISABEL RAMOS MARQUES

BSc in Biomedical Engineering

Adviser: Dr. Ana Catarina Bernardino Baptista,
Researcher, NOVA University Lisbon

Co-Adviser: Dr. Isabel Maria das Mercês Ferreira,
Associate Professor, NOVA University Lisbon

Examination Committee:

Chair: Dr. Ricardo Nuno Pereira Verga e Afonso Vigário,
Associate Professor, NOVA University Lisbon

Rapporteurs: Dr. Célia Maria Reis Henriques,
Associate Professor, NOVA University Lisbon

Adviser: Dr. Ana Catarina Bernardino Baptista,
Researcher, NOVA University Lisbon

MASTER IN BIOMEDICAL ENGINEERING

NOVA University Lisbon
April, 2024

Electro-responsive on-demand drug delivery system for e-Patches

Para as minhas pessoas,
as que estão, e as que gostava que estivessem.

ACKNOWLEDGMENTS

A concretização da presente dissertação marca não só o fim de um último ano de aprendizagens, como também culmina no encerrar de uma etapa de cinco anos, marcada por uma infindável coleção de vivências mas acima de tudo, por pessoas que a acompanharam. Se este for o momento em que consigo agradecer a cada uma delas, resta-me o esforço de que estas palavras cumpram o seu objetivo escrito.

Em primeiro lugar, expressar um agradecimento profundo às pessoas que me orientaram e guiaram nos últimos meses, e com quem tive o prazer de aprender diariamente. Agradecer pela oportunidade de emergir neste projeto e nestes laboratórios, sempre cheios de um espírito de cooperação inspirador. À minha orientadora, Professora Doutora Ana Baptista, agradecer pelo apoio desde o primeiro dia, pelo incentivo, pela flexibilidade, por me ter dado a confiança que precisei quando duvidei dela, pela gentileza sempre presente, por todos os momentos de brainstorming e de resolução de dúvidas, e por ter sempre agilizado um tempinho extra para que houvesse espaço para elas, às vezes sei que em circunstâncias difíceis. Um agradecimento por me ter feito perceber que "fazer ciência" passa também por desenvolver um olhar sobre alguma coisa, e procurar olhar para lá dela, porque para além de possíveis respostas teóricas, trata-se também de uma questão de curiosidade e de experiência e do poder da não desistência à primeira tentativa. À minha coorientadora, Professora Doutora Isabel Ferreira, por toda a prontidão na partilha de ensinamentos e por todo o conhecimento que me fez chegar. Pela simpatia, por me ter recebido e integrado tão bem, e pelo tempo que me dedicou. À pessoa que nunca me fez sentir perdida dentro do laboratório, o Miguel, a quem agradeço também por toda a ajuda do início até ao fim da minha jornada aqui, pela discussão de ideias e hipóteses, pela motivação que sempre me fez chegar e pelos conselhos que me deu. A todas as pessoas que conheci e com quem me cruzei aqui, obrigada por todo o companheirismo e por me terem ensinado alguma coisa.

Às três pessoas que caminharam de mão dada comigo diariamente por estes cinco anos fora. Ao Luís, à Mariana, à Margarida. Pela partilha das memórias mais felizes que vivi aqui mas também por me incentivarem a continuar e a ir mais além nos momentos mais sofridos, que também fizeram parte da viagem. Não sei se teria chegado aqui sem vocês ao meu lado, mas sei que na hipótese de o ter conseguido, não teria sido com a mesma felicidade, vivacidade e intensidade. Tornaram estes anos em algo muito especial para mim, e marcaram o meu crescimento, e por isso e pela amizade sincera que sempre senti que partilhámos, e partilhamos, estarei sempre agradecida. Obrigada por terem olhado sempre por mim.

Às amigas que têm crescido comigo pelos diferentes ciclos pelos quais a vida se vai construindo. À Mariana B, à Mariana G, à Irina. Às amigas que levarei sempre num lugar especial por tudo o que já vivemos. À Bia, à Casca. São a minha prova viva de que a amizade não precisa de ser uma contínua vivência de momentos no presente, para continuar a ter o seu valor. Pela beleza que estas amizades têm em mim, por saberem viver e crescer a uma pequena distância conhecida, sabendo sempre onde se cruzar. Obrigada pelo apoio, por acreditarem sempre em mim, por terem cá estado, e pela amizade que tenho a sorte de poder partilhar com cada uma de vocês.

Aos amigos que são a minha segunda família. Ao Buzz, ao Dinis, ao Fonsi, ao Fran, ao Gui, à Juca, à Martinez, à Nokas, ao Pedrocas, ao Roman, ao Sebas. Obrigada por tornarem esta coisa de crescer mais fácil e imensamente bonita. Obrigada por fazerem parte das melhores memórias que tenho comigo, por estas ligações não muito fáceis de encontrar na vida, que existem entre nós. Um obrigado a cada um por me terem acarinhado nos dias mais desafiantes e turbulentos e por melhorarem cada metamorfose da minha vida. Acreditem sempre em vocês porque têm a magia de construir coisas grandes e bonitas, pelas pessoas grandes e bonitas que são, na vossa totalidade. Ao Buzz, obrigada por me fazeres escolher o melhor Bloco Livre da FCT. Ao Fonsi, obrigada pela ajuda no AutoCAD na construção do melhor dedo da história das próteses. Ao Fran, obrigada pelo livro sobre como programar em C e pelas horas que tiraste para ma explicar. Ao Gui, obrigada pelas horas na Biblioteca do Seixal a elucidares-me sobre Contabilidade. À Martinez, obrigada pelos 20 PPTs de teoria de programação que me fizeram passar a Introdução à Programação B. Ao Pedrocas, pelo empréstimo da sebenta de 400 páginas de Eletromagnetismo e pelo teu highlight de resumo nas 40 mais importantes. Ao Roman, por ter sido explicador de Biofísica, Biomecânica, Química B, Análise I, II, III, IV (?). Ao Sebas, pelo conforto e pela companhia através da sua arte de fazer música, a qual apreciei e absorvi em todas as fases deste meu percurso, pela qual estendo o meu obrigada ao Vasco e ao Tomás.

À Juca, por editar de mão dada comigo pela madrugada fora, o melhor vídeo-projeto de Biologia Celular e Molecular, e por me ter relembrado sempre que precisei, de que de facto, só vivemos uma vez. À Nokas, pelos apontamentos mais bonitos alguma vez produzidos de Microeconomia, de Álgebra, de Física II, de Análise I, II, III (?), e por me ter relembrado sempre que precisei, de que há sempre a hipótese de uma visão de um copo meio cheio sobre quase tudo na vida. A vocês as duas, obrigada por existirem como duas segundas irmãs na minha vida, pelo conforto que me trazem e pelo apoio em tudo o que vivi nestes anos e pelo que vá viver. Não sei se juntos formamos uma equipa muito completa, ou se o meu curso é demasiado abrangente, mas agradeço a cada um por terem contribuído para o meu sucesso a curto e a longo prazo.

Ao Dinis, a quem sinto que devo a indexação de um novo parágrafo. Na continuação, agradecer primeiro pelas macros daquele Excel. Depois agradecer-lhe por ser alguém formado em Gestão diariamente pronto a ouvir sobre os meus avanços e recuos na Ciência, e surpreendentemente percebê-los, porque tenho em mim a certeza de que nesta altura do campeonato ele já conseguia fazer um pitch (melhor ou pior) sobre cada uma das keywords desta dissertação. Agradeço pelo sentimento de leveza que me trouxe, pela felicidade que me traz, e por ser alguém que admiro e me inspira, trazendo à tona a minha melhor versão. E porque à distância de 10 minutos de carro (às vezes 8) ou à distância de 3 horas de avião (às vezes 14), esteve continuamente presente, e teve lugar cativo na arte de conseguir diminuir todas as minhas tempestades, e de relembrar-me de que fazem parte natural de um caminho. Agradeço pelo apoio, agradeço pelo amor, e agradeço por ter acompanhado o meu percurso de estudante desde que, na verdade, dei os meus primeiros passos nele.

Por último, um especial obrigado à minha família. Ao meu mano, por ser a pessoa que tanto acredita em mim, que tenho o prazer de crescer com, que tanto zela por mim, que transforma as minhas vitórias nas suas maiores vitórias e que tem sempre as palavras mais bonitas para me oferecer. Aos meus pais, por me terem permitido chegar até aqui e por terem caminhado sempre ao meu lado, que será sempre dos maiores privilégios que vou ter na vida. Por celebrarem comigo as minhas concretizações, por me encorajarem a não desistir das minhas metas, mesmo nos momentos mais desafiantes, por não deixarem de me aturar nos meus dias mais difíceis, por se preocuparem e se importarem. E sobretudo, por terem esculpido a pessoa que sou, pelos valores que me fizeram chegar, por me mostrarem que a vida é sobre pessoas e aquilo que com elas criamos, por poder chegar ao fim desta etapa com estas pessoas a quem não podia deixar de expressar o meu agradecimento, e por vocês também terem sempre escolhido fazer parte da vida delas.

Este trabalho foi realizado no âmbito do projeto "All-Fiber Integrated Photovoltaic Storage Devices for e-Textiles" de referência PTDC/CTM-CTM/157/2020, financiado por fundos nacionais via FCT, IP.

"Temos de olhar para lá das coisas,
como se elas fossem de vidro.
Cada coisa que existe neste mundo é transparente,
mas nós teimamos em vê-las opacas.

As coisas são janelas de vidro
que dão umas para as outras,
umas para dentro das outras.
Cada coisa é uma porta
que dá para uma porta."

Em "Para Onde Vão os Guarda-Chuvas", de Afonso Cruz

Abstract

Controlled drug delivery technologies represent a significant advancement in modern pharmacotherapy, offering distinct advantages over traditional drug delivery systems. Unlike traditional methods, where drugs are often absorbed by various parts of the body before reaching the intended treatment location, resulting in the need for higher drug concentrations and potentially causing adverse effects, controlled-release systems emerge to overcome these limitations. Therefore, to address these shortcomings, this study explores a drug delivery system with conductive polymers for electrical stimulus responsiveness, by employing non-invasive, externally controlled drug release mechanisms, for topical applications. Incorporating electrical stimulation ensures a more timely and effective response to treatment - this type of stimulation allows for dynamic control over drug release kinetics, by modulating the electrical signals and enabling tailored dosing regimens based on individual patient needs, while minimizing systemic exposure. Electrospun cellulose acetate fibers impregnated with a cationic drug were functionalized with polypyrrole and poly(3,4-ethylenedioxythiophene) to enable electrical stimulation. Results revealed that negative potentials enhanced the release of this positively charged drug molecule through the fibers, while positive potentials had the opposite effect. Consequently, the conducted study demonstrates the influence of electrical stimulus type and the charge of the selected model drug on release profiles and allows to contribute to the development of more personalized and efficient therapies in long-term dermatologic diseases, ultimately improving patient outcomes and enhancing their quality of life.

Keywords: Controlled drug delivery systems, electrospinning, cellulose acetate, conductive polymers, polypyrrole, PEDOT, electrical stimulation

RESUMO

As tecnologias de libertação controlada de fármaco representam um avanço significativo na farmacoterapia moderna, pelas vantagens que apresentam sobre os sistemas tradicionais de entrega de fármacos. Ao contrário destes métodos tradicionais, nos quais os medicamentos são absorvidos por várias partes do corpo até atingirem o local de tratamento pretendido, resultando na necessidade de concentrações mais altas de medicamentos e consequentes efeitos adversos, os sistemas de libertação controlada superam estas limitações. Desta forma, este estudo explora um sistema de entrega de fármacos com polímeros condutores que respondem a estímulos elétricos, através de mecanismos de libertação não invasivos e controlados externamente, para aplicações tópicas. A estimulação elétrica garante uma resposta mais rápida e eficaz ao tratamento - este tipo de estimulação permite o controlo dinâmico sobre a cinética de libertação dos medicamentos, modulando os sinais elétricos e possibilitando regimes de dose personalizados com base nas necessidades individuais dos pacientes, enquanto minimiza a exposição sistémica. Assim, fibras de acetato de celulose produzidas por electrofiação foram incorporadas com um fármaco de carga positiva e funcionalizadas com polipirrol e poli(3,4-etilenodioxitiofeno) para permitir a estimulação elétrica. Os resultados revelaram que os potenciais negativos aplicados resultaram num aumento da libertação das moléculas deste fármaco pelas fibras, enquanto potenciais positivos tiveram o efeito oposto. O estudo conduzido demonstra assim a influência do tipo de estímulo elétrico aplicado e da carga da molécula dos fármacos selecionados nos perfis de libertação destes sistemas e permite contribuir para o desenvolvimento de tratamentos mais personalizados e eficientes contra infeções dermatológicas prolongadas, melhorando assim a qualidade de vida dos pacientes.

Palavras-Chave: Sistemas de libertação controlada de fármaco, acetato de celulose, polímeros condutores, polipirrol, PEDOT, estimulação elétrica

CONTENTS

LIST OF FIGURES

List of Tables

ABBREVIATIONS

ATR	Attenuated Total Reflectance
CA	Cellulose Acetate
CP	Conductive Polymer
CV	Cyclic Voltammetry
DMAc	Dimethylacetamide
$FeCl_3$	Iron (III) chloride
FTIR	Fourier Transform Infrared Spectroscopy
IBU	Ibuprofen
MB	Methylene Blue
NPs	Nanoparticles
OM	Optical Microscopy
PEDOT	Poly(3,4-ethylenedioxythiophene)
PPy	Polypyrrole
SBF	Simulated Body Fluid
SEM	Scanning Electron Microscopy

1

INTRODUCTION

1.1 Motivation and Context

Transdermal drug delivery systems currently represent an area of innovation with a significant role in human health. They offer not only the advantage of non-invasive and effective drug administration but also demonstrate results that support increased therapeutic efficacy in various diseases. In recent decades, numerous studies have emerged on these systems, ranging from new methods of controlling drug release to various types of polymeric substrates and incorporated drugs. The advent of conductive polymers and electronic control has enabled concrete scientific advancements in controlled drug release. Electrical stimulation has shown great potential in the treatment of prolonged dermatological conditions as it can provide the precise dosage of an active substance based on individual needs.

At the same time, achieving an ON/OFF type of stimulus-controlled release profile with a device entirely based on fibers able to breathe freely and capable of accommodating different electro-mechanical deformations remains challenging. Only through complete control of the release rate is it possible to maintain drug concentrations within the appropriate thresholds for effective and personalized medical treatment for each patient. It is with these objectives in mind that this study emerges. Therefore, it is expected that this research will contribute to the ongoing innovation in this scientific and technological field.

The research work described in this dissertation was carried out in accordance with the norms established in the ethics code of Universidade Nova de Lisboa. The work described and the material presented in this dissertation, with the exceptions clearly indicated, constitute original work carried out by the author.

1.2 Transdermal Drug Delivery Systems

Transdermal drug delivery systems have been studied over the last few decades as a novel approach to addressing the issues associated with conventional drug administration routes. The first transdermal patch was approved by the Food and Drug Administration approximately 40 years ago, and since then, numerous studies and innovations have emerged and been applied to these systems, as evidenced in Bird et al.'s review article from 2020 [1].

A transdermal drug delivery system is a method of administering medications through the skin using adhesive patches or similar formulations. This non-invasive system allows for the controlled release of drugs directly into the bloodstream, providing steady therapeutic levels over extended periods and enhancing bioavailability by bypassing the gastrointestinal tract and first-pass metabolism. These systems improve patient compliance through ease of use, making it particularly beneficial for chronic conditions requiring long-term medication, and have witnessed significant scientific advancements and exponential growth in the development of innovative and efficient systems, capable of overcoming limitations imposed by conventional drug administration methods such as oral and injectable routes. In such systems, the amount of medication that reaches the target tissue is much lower than the administered dose, as it is gradually absorbed by various tissues in the body before reaching the target tissue, and the drug itself undergoes degradation [2]. Consequently, a higher drug dose is required to achieve the desired effect, thereby increasing potential side effects in patients. Controlled drug release systems emerge as a solution to address these issues, primarily by avoiding overdosing and associated toxicity in the body [3]. Additionally, transdermal delivery is a simple and painless procedure that can often be self-administered, thereby enhancing patient adherence to the therapy in question [4].

In conventional drug delivery systems, the drug level is not maintained within the therapeutic window, which poses a significant limitation. After the administration of a single drug dose, it metabolizes rapidly, resulting in a sharp increase in its concentration, immediately followed by an exponential decrease. As a result, the absorption period of the drug in the target tissue is not sufficiently prolonged, leading to a subtherapeutic response. To compensate for this, multiple doses of the drug are administered, often at higher levels, which can introduce toxicity into the body [2].

Various approaches have been studied to maintain drug concentrations above the minimum effective level and below the toxic concentration. The development of controlled release systems provides a solution to this problem.

1.3 Electrospinning

In recent years, the use of polymeric nanofibers produced through the electrospinning process has proven to be an effective method for producing fibers as a support for bioactive substances in drug delivery systems. These fibers possess noteworthy features such as high surface area-to-volume ratio and open porous structures [5]. Furthermore, the fact that different types of therapeutic agents can be encapsulated or surface-conjugated within the fibers, turn them promising in several drug delivery applications, such as the delivery of anti-inflammatory agents, as studied by Kotroni et al. in 2019 [6], antibacterial agents, as proven in Gouda et al.'s study from 2014 [7], as well as amino acids and vitamins, as demonstrated in Taepaiboon et al.'s research from 2007 [8]. Due to being easily surface-functionalized, having tailorable morphologies and inherently resembling natural extracellular matrix, which is advantageous for cell attachment, proliferation, and differentiation, nanofibers are distinguished from other drug delivery devices, such as nanoparticles or hydrogels [9] .

In the electrospinning process, a high voltage is applied between a polymeric solution and a grounded collector. The solution is fed into a syringe and placed on a syringe pump. When a sufficiently high voltage is applied, the particles in the solution become charged and repeal each other. When the electrostatic forces reach values comparable to the surface tension forces, the droplet takes the form of a cone, also known as Taylor's Cone. Once the electrical field intensity is high enough, the electrostatic forces overcome the polymeric solution surface tension, and a polymeric high-speed jet is ejected through the tip of a needle towards the collector at a controlled flow rate. Along its trajectory, the solvents evaporate, allowing the polymer to be deposited as fibers with diameters ranging from micrometers to nanometers, with adjustable mechanical properties [10]. Various parameters influence the transformation of polymeric solutions into fibers and can affect its characteristics, as described in the systematic review of Jain et al. [11]. These parameters are related to the properties of the polymer solution used, such as concentration and viscosity, the molecular weight of the polymer, its conductivity, and surface tension; to process variables like the flow rate and the electric potential at the needle, and the distance to the target (distance between the needle tip and the metallic collector); and to environmental parameters, such as the temperature of the electrospinning chamber and the humidity inside it. Taking these parameters into account and optimizing them during the electrospinning process is essential to achieve the desired nanofiber properties and functionality. Thus, electrospinning technique encompasses a complex interplay of parameters crucial for controlling nanofiber morphology and structure.

Cellulose Acetate (CA) stands out as a significant biopolymer that is currently gained attention in drug delivery systems due to its biocompatibility, low cytotoxicity, and the exhibition of excellent ionic conductivity [12]. CA electrospun nanofibers have thus attracted considerable interest in a wide range of clinical applications including the delivery of drug molecules to local treatment as patches through the skin, producing effective healing, as demonstrated in the study by Khoshnevisan et al. [13], used as implants to prevent post-surgical adhesions and infections, with antibacterial applications, as reported by Jatoi et al. [14], used for wound dressings, as proved in the study by Khan et al. [15] , and are also used to build scaffolds for tissue-engineered constructs, as investigated by Liang et al. [16]. For these reasons, CA fibers are desirable for drug delivery, and it was the polymer chosen to produce electrospun fibers for the proposed device in this thesis.

1.4 Conductive Polymers

Despite these advancements, traditional transdermal drug delivery systems materials show static features for drug-releasing with a therapeutic effect that is dependent on the limited drug dosage and dosing interval. In other words, once the drug is administered there is no further control over release characteristics. Consequently, transdermal drug delivery technology has progressed from passive release mechanisms (without external energy input) to active release methods that respond to external stimuli. Understandably, a growing body of research has raised the importance of developing sophisticated drug delivery systems to improve the dynamic responsiveness of biomaterials, with better control over drug release in which both the rate and the amount of the active substance are precisely tailored to meet specific needs [17]. Therefore, external stimulating signals, such as temperature (Gandhi et al. 2015 [18]), magnetic (Sharma et al. 2020 [19]), electrical (Servant et al. 2013 [20]), optical (Liu et al. 2017 [21]), and internal stimulating signals, such as pH (Qu et al. 2018 [22]) can be used to trigger and/or control drug release and achieve the purpose of drug administration on-demand. The above-mentioned studies are examples that show the feasibility and potential of applying external stimuli to control drug release rate. Among them, the electrical stimulation, which is the external stimuli focused on the present study, offers some advantages over other types of stimuli, and has attracted attention since electrical signals are easily controlled so that can allow repeatable and reliable drug release for clinical needs and can be precisely adjusted and controlled using voltage or current amplitude and pulse duration [23].

In recent decades, the primary classes of electro-responsive controlled release systems that have been developed are electro-responsive hydrogels, electro-responsive layer-by-layer films, and conductive polymers (CPs). Conductive polymers, when electrically stimulated, can release charged drugs through partial oxidation or reduction [24]. The inherent conductivity of CPs is the result of the polymer molecule comprising a conjugated chain of localized carbon–carbon single bonds (σ) and localized carbon–carbon double bonds (π), as illustrated in Figure 1. When the p-orbitals overlap in the π bonds, the electron movement between atoms becomes better, allowing the electrons to move along the polymer chain. The higher conductivity of polymers is further based on the incorporation of dopant ions balancing the charge introduced through oxidation (p-doping) or reduction (n-doping). The dopant introduces a charge carrier by removing/adding electrons from/to the polymer chain [25]. Therefore, the focus of this study applies upon the functionalization of CA membranes using conductive polymers to achieve specific controlled release behavior.

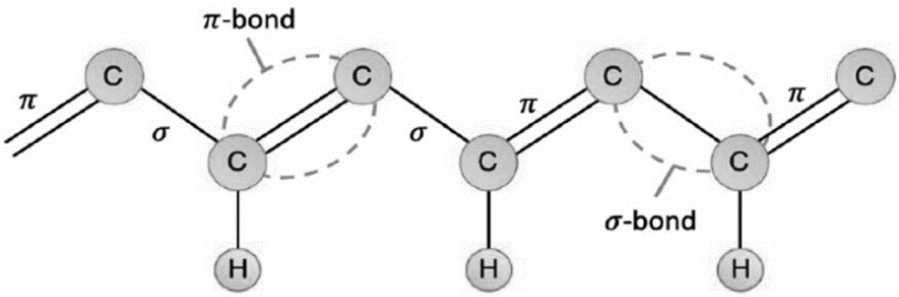

Figure 1: Scheme of a conductive polymer conjugated backbone. (Adapted from [23])

Currently, polypyrrole (PPy) and poly(3,4-ethylenedioxythiophene) (PEDOT) are among the most widely explored conductive polymers for biomedical applications: in the field of tissue engineering, Maharjan et al. in 2020 [26], developed a method to embed polypyrrole nanoparticles (PPy-NPs) into a polymeric matrix through in-situ polymerization, creating conductive scaffolds. These scaffolds exhibited enhanced mechanical strength, conductivity, biomineralization, and cell adhesion, suggesting their potential for bone tissue engineering applications. In the area of neural regeneration, Zhao et al. in 2020 [27] investigated the effects of electrical stimulation delivered through implanted PPy/Silk Fibroin composite scaffolds in rat sciatic nerves. Their findings revealed that electrical stimulation facilitated axonal regeneration and functional nerve restoration without eliciting any inflammatory response, showcasing the

potential of conductive polymer-based scaffolds for neural regeneration applications. As well as in biosensors, a novel electrochemical biosensor was developed by Liu et al. in 2018 [28] using a biohybrid conducting polymer, integrating glucose oxidase and PEDOT microspheres. This biosensor showed superior glucose sensing performance, with a wide linear range, high sensitivity, and excellent storage stability, indicating its potential for practical applications in biosensing and bioelectronics.

Oxidative polymerization of monomer units can be achieved via chemical or electrochemical redox polymerizations [29]. In this study, two different in-situ chemical polymerization processes were conducted for the synthesis of PPy and PEDOT: aqueous solution polymerization for PPy and vapor phase polymerization for PEDOT. The chemical structures of these two conductive polymers are represented in Figure 2.

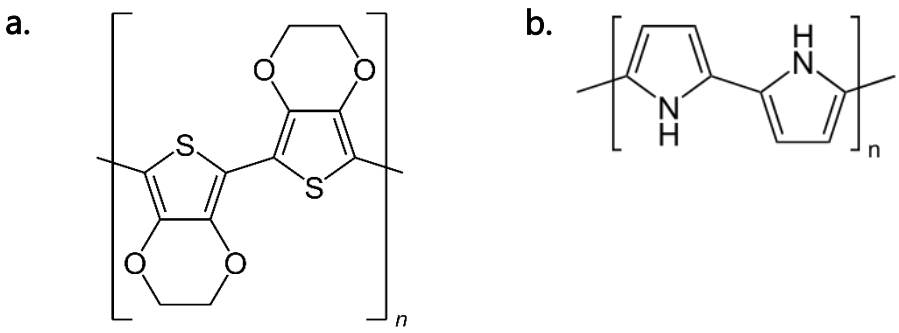

Figure 2: Chemical structure of PEDOT (a) and PPy (b). (Adapted from [23]).

PPy can be obtained through chemical polymerization of pyrrole in liquid phase, that occurs by adding pyrrole monomers to an aqueous solution with an oxidizing agent. In this mechanism, the initial step involves the production of a positively charged free radical through the oxidation of pyrrole monomers, which is unstable and highly reactive, and allows for the formation of a neutral dimer. As this compound is also oxidative, it combines with other monomers through the same process, thus creating the polypyrrole chain. In this in situ oxidation, the polymer remains in its oxidized state and the conducting characteristics of the polymer result from the Cl^- ions in its chain constitution.

The schematic mechanism of oxidation of pyrrole with $FeCl_3$ is represented in Figure 24 of Appendix A. The electrical conductivity is affected by a variety of factors, among which are the choice of solvent and oxidant agent, the pyrrole/oxidant agent ratio, and the duration and temperature of the reaction [30].

PEDOT synthesis through oxidative chemical polymerization is similar to the respective polymerization principle of PPy. In this case, the vapor phase polymerization of EDOT involves coating the surface of the substrate with the oxidizing agent, followed by exposure to a controlled atmosphere of CP monomer vapors. The schematic representation of vapor phase polymerization of EDOT is illustrated in Figure 25 of Appendix A. The parameters controlled during this polymerization process include monomer concentration, substrate temperature, and polymerization time [31].

These two CPs are also suitable and effective for drug delivery systems that require the release of active substances upon electrical stimulation due to their unique electrical and physicochemical properties as Abidian et al. [32], Müller et al. [33], Esrafilzadeh et al. [34], Tang et al. [35] demonstrated. They possess good biocompatibility, biodegradability, and low toxicity. In addition, have high surface area, good charge storage capacity, and the highest conductivity. Therefore, several studies have emerged to continually investigate the potential of PPy and PEDOT for precise and on-demand drug release:

In 2006, Wadhwa et al. [36] developed one of the first electronically controlled drug delivery systems. This system consists of two electrodes on which a PPy film is deposited to achieve controlled and localized delivery of dexamethasone (anti-inflammatory anionic drug) that is incorporated into PPy through electro-polymerization of pyrrole. Dexamethasone, due to its negative charge, acts as a dopant for the conductive polymer. The drug release was performed using cyclic voltammetry (CV) between -0.8V and +1.4V in a PBS (Phosphine Buffered Solution) medium, and it was observed that from the third cycle of scanning, characteristic peaks of pyrrole oxidation and reduction emerged. Furthermore, it was possible to conclude that with more cycles, the peaks became more intense, and additionally, the drug release did not produce any toxic side effects.

In 2014, Krukiewicz et al. [37] studied the release of ibuprofen (IBU) in its anionic form encapsulated in a PEDOT film, through the application of electrical stimuli. They conducted too the CV technique, with potentials between -0.8V and +0.8V to observe the drug release profile in a PBS medium. The results demonstrated that the maximum amount of IBU released corresponded to an electrical potential of -0.5V, and without applied potential, the release was six times lower than at the mentioned potential. Potentials lower than -0.5V and close to positive values resulted in a decrease in concentration of released ibuprofen caused by the effect of n-doping of negatively charged polymer matrix with cations present in PBS solution: the incorporation of potassium cations occurs instead of the release of the anionic form of IBU. The concentration of IBU released decreases as the value of applied potential increases since the

positively charged film holds the anionic drug. Based on these results, they concluded that the application of negative potentials results in facilitated release of the anionic drug used as a co-dopant, IBU, while the application of positive potential results in the drug retention.

In 2019, Boehler et al. [38] demonstrated that controlled release can be achieved by combining certain specifications of drug delivery systems. In this study, they added dexamethasone to PEDOT and deposited this substrate in the form of films on two iridium oxide electrodes. For different film thicknesses, they applied different types of electrical signals: cyclic voltammetry and continuous potential. They observed that in passive diffusion tests, there was a substantial amount of drug being released into the medium over time. In active tests, they tested the three mentioned signal types and found that for the cyclic voltammetry signal (with potentials between -0.6V and 0.9V), there was considerable drug release into the medium, similar to passive release. They also found that with a continuous potential stimulus of -0.6V, drug release into the medium was limited, resulting in a different release profile compared to diffusion and cyclic voltammetry.

1.5 Model Drug

Several studies have investigated different strategies to explore drug release mechanisms and to incorporate the different types of ionic drugs - cationic and anionic. The final effect of electrical stimulation on drug release depends on how the CP responds to the stimulus, how the drug is released from the polymeric fiber due to electrostatic forces and its physicochemical properties, and how the interactions between the CP and the drug influence the process. Therefore, the release process of drug molecules from CPs has been under study in recent years, relying on a combination of electro-chemo-mechanical action in CPs leading to drug release [39].

In 2021, Baptista et al. [3] studied the electronically controlled release of ibuprofen impregnated in gauze membranes and AC fibers. They obtained conductivity values in the range of 1-10 mS/cm in PPy-functionalized gauze, providing controlled drug release in a system composed of PPy/Ibuprofen/PPy and a silver electrode. The results demonstrated PPy adherence to the fibers and confirmed the incorporation and release of the drug. A small dermal patch constructed with these membranes retained ibuprofen at 1.5V and released it rapidly upon application of -0.5V. In 2022, this study was continued [40], exploring functionalization with PEDOT and the directly addition of ibuprofen within the electrospinning process. Using alternating voltages, an ON/OFF release profile was achieved for all systems proposed and

these conditions were successfully replicated in a prototype transdermal patch containing the membranes, a thin silver wire, and covered with a clean dressing to simulate possible skin contact.

The present work aims to continue this research based on its positive and promising results. The goal is to investigate how the electrically stimulated release system works with a drug of different charge than ibuprofen: thus, methylene blue (MB), a cationic compound, was used as a model to simulate the release of a positively charged drug in this type of system and consequently studying its release profile and comparing it with the negatively charged drugs already studied in the previous research.

The chemical structure of the molecule is represented in Figure 3. MB has been recently used as cationic model drug in drug delivery systems, as reported by Ding et al. [41] with the development of an electro-responsive layer-by-layer film, and by Gao et al. [42] with a microgel-based reservoir device.

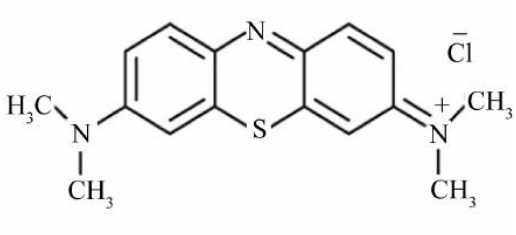

Figure 3: Chemical Structure of MB. (Adapted from [43]).

Studying and comparing the results of drug delivery systems controlled by electrical stimulation, with both positively and negatively charged drugs offers several advantages - it enhances our understanding of the underlying mechanisms, expands the selection of drugs for potential use, enables tailored delivery based on drug properties, optimizes electrochemical parameters, and provides a comprehensive evaluation of efficacy and safety. By exploring both types of charged drugs, researchers can refine these systems to achieve improved therapeutic outcomes across various biomedical applications [39]. In this context, the development of this drug delivery emerges in this study, with three main objectives in mind: the production of CA fibers through the electrospinning technique, and the encapsulation of the model drug within these fibers, the functionalization of drug-containing fibers using PPy and PEDOT as conductive polymers and the validation of the electrically tunned drug delivery platform under several electrical conditions in a simulated body fluid solution.

Through the above-mentioned studies, it is evident that there are numerous advantages and developments around electronically controlled drug delivery systems. At the same time, there is still room for growth and innovation in these systems to make them more user-friendly through increasingly intelligent technologies [44], [45], and improve patient adherence, especially in geriatric care, where their need is particularly important. In this field, regular topical administration of drug for skin diseases is perhaps one of the main needs. By combining sensors and external communication, these systems can offer patients an autonomous, and intelligent way to administer medication for remote treatment, as well as on-demand precision medicine, as described in the systematic review carried out by Vadlapatla et al. [46].

2

EXPERIMENTAL SECTION

This chapter addresses the experimental details and procedures carried out for the development of the proposed biodevice. Thus, the following steps are outlined: production of membranes through electrospinning technique (section 2.1), their functionalization with PPy and PEDOT (section 2.2), and morphological, chemical, electrical, and electrochemical characterization methods (section 2.3). The procedure for electrical stimulation and consequent release of the encapsulated model drug is presented in last section (section 2.4).

2.1 Production of Membranes

In this study, both cellulose acetate polymeric membranes (CA) and cellulose acetate polymeric membranes with encapsulation of the model drug (MB:CA) were produced using electrospinning technique.

2.1.1 Polymeric Solutions

CA (Mn 50,000 with 39.7% acetyl groups, Sigma Aldrich) fibers were produced using a polymeric solution of 12% w/t in a binary solvent system of acetone (99.5%, Honeywell Riedel-de Haën) and dimethylacetamide (DMAc) (Carlo Erba Reagents S.A.S.), with a ratio of 2:1, respectively. Thus, an amount of 1.2 g of CA was added to a volume of 10.6 mL of the binary solvent system. This dissolution took place under constant magnetic stirring at 100 rpm, at room temperature and humidity. The solution was left under constant magnetic stirring until the cellulose acetate was completely dissolved, resulting in a visibly homogenized, translucent solution with the absence of solid particles in suspension.

MB compound ($C_{16}H_{18}ClN_3S$, High Purity, Mw=319.85 g/mol, Thermo Scientific Chemicals) was added to a CA solution to produce fibers with the model drug compound selected for this study (MB:CA). A CA polymeric solution of 10% w/t was prepared with the same binary solvent system of Acetone-DMAc in a ratio of 2:1. Thus, an amount of 1 g of CA was added to a volume of 10.8 mL of the binary solvent system, in which 25 mg of MB (according to the solubility of MB in acetone at 25ºC [47]) were added.

2.1.2 Electrospinning

For the electrospinning process, a volume of 1mL of the homogenized solutions were added to a syringe (B. Braun) with a metallic needle of 21 gauge (internal diameter of 4.5 mm from ITEC, Iberiana Technical) and placed in an infusion syringe pump (NE300 from New ERA Pump Systems) to control the flow rate that the polymeric solution was ejected during the process. A high voltage source (incorporated in a modular robotic system, LRC MultiCoater) was used to apply a high voltage to the metallic tip, and a grounded static collector (metallic foil) was placed at a certain distance from the needle. A schematic setup of this process is illustrated in Figure 4.

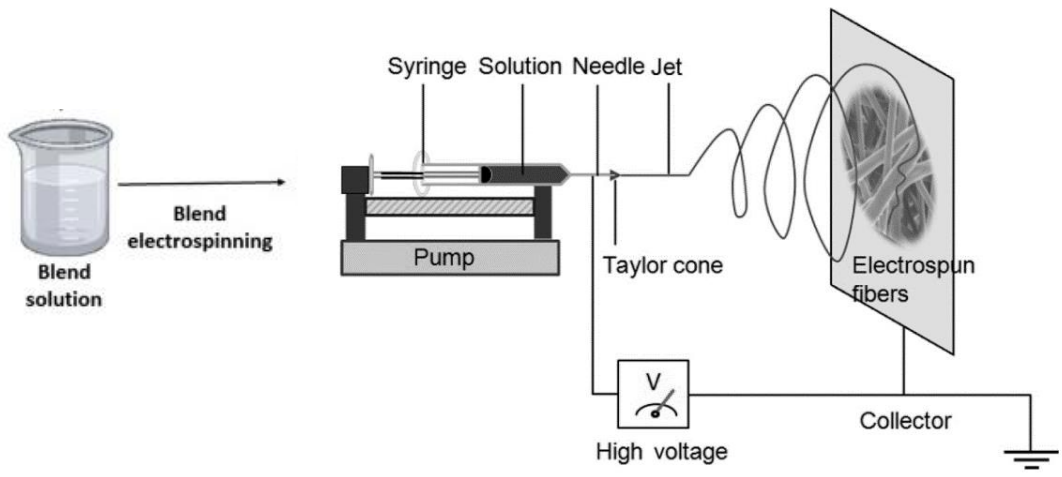

Figure 4: Electrospinning setup. (Adapted from [9]).

Table 1 describes the parameters that were defined and regulated for the electrospinning of CA and MB:CA fibers, based on the study of Baptista et al. from 2018 [48].

Table 1: Summary of the electrospinning parameters used to produce CA and MB:CA membranes.

	Collector Distance (cm)	Voltage (kV)	Flow Rate (mL/h)	Humidity (%)	Temperature (ºC)	Deposition Time (h)
CA	20	18	0.2	35-45	20-25	5
MB:CA	15	20				

Given that the deposition time was 5 hours at a flow rate of 0.2 mL/h, each electrospun membrane contained 1 mL of polymeric solution, with an approximate amount of MB equal to 2.3 mg. To achieve a similar amount of MB in all sample portions, the electrospun membranes were cut into eight similar concentric triangles. Therefore, assuming that the mass of MB is uniformly distributed throughout the membrane, each of these triangular membranes contained approximately 0.3 mg of MB.

2.2 Functionalization of Membranes

In order to ensure the electrically conductive character of the fibers, CA and MB:CA membranes were coated with the chosen CPs for this study (PPy and PEDOT), through the functionalization of the electrospun fibers' surface.

2.2.1 Liquid Phase In Situ Polymerization of Pyrrole

CA and MB:CA triangular membranes were immersed in a volume of 10 mL of an aqueous solution of 0.05 mol/L pyrrole (98%, Sigma-Aldrich) and stirred for 10 minutes at room temperature, allowing the impregnation of the pyrrole monomer. After this period, a 10 mL solution of the oxidizing agent, iron (III) chloride hexahydrate ($FeCl_3.6H_2O$, purity 99%, Chem-Lab NV) was gently added in a mass ratio of 2:1 ($FeCl_3$:Pyrrole) [48]. During the oxidative polymerization of pyrrole, CA and MB:CA membranes changed from white or blue to black, respectively, confirming the formation of PPy. After the polymerization time intervals, CA and MB:CA membranes were carefully removed from the solutions and washed with ultrapure water (Elix®

purification system, Merck Millipore) and ethanol (99.5%, Honeywell Ricomel-de Haën) to remove the by-products and unreacted residues, and were dried at room temperature. A schematic setup of this functionalization process is illustrated in Figure 26 of Appendix B.

2.2.2 Vapor Phase Polymerization of EDOT

EDOT functionalization process of the CA membranes through exposure to EDOT vapors, was based on an experimental procedure adapted from the literature [49]. The electrospun membranes were immersed in a 40 g/L aqueous solution of an oxidizing agent, iron (III) chloride hexahydrate ($FeCl_3.6H_2O$, purity 99%, Chem-Lab NV), in a volume of 10 mL, for 20 minutes under 100 rpm stirring. After this period, the membranes impregnated with the oxidizing agent were carefully removed from the solution and left to dry at room temperature for 60 minutes. Once dried, they were fixed inside a closed chamber with 0.5 mL of the EDOT monomer (97%, Mw=142.18 g/mol, Sigma-Aldrich) at the bottom of the container. The chamber was placed in an oven (Memmert, Schwabach) at 90ºC and the exposure time of the membrane to monomer vapors was exclusively evaluated for 120 minutes, as illustrated in Figure 27 of Appendix B. During this EDOT polymerization, the membranes changed from white to black, indicating the formation of PEDOT. The coated membranes were removed from the chamber and washed with ultrapure water (Elix® purification system, Merck Millipore) and ethanol (99.5%, Honeywell Ricomel-de Haën) to remove by-products and unreacted oxidant and monomer. The samples were dried at room temperature.

An experimental study, illustrated in Table 5, in Appendix C, was conducted to optimize the PEDOT functionalization process in MB:CA membranes. Under the initial conditions used for CA membranes polymerization, the membranes impregnated with methylene blue became brittle and prone to fragmentation upon removal from the oven. Consequently, some adjustments were implemented: the oven temperature was lowered to 75ºC, and 1 mL of distilled water was added to the 0.5 mL of EDOT. These modifications successfully eliminated the brittle character of the membranes.

2.2.3 Membrane Systems

Four different membrane systems were considered, as described in Table 2. The single systems consist of only one membrane, whereas the multi-layered systems are composed of three layers, with drug incorporation occurring within the inner layer. The layered systems were sealed with adhesive tape (Kapton® tape, DuPont) to ensure that passive release doesn't occur from the edges through diffusion.

Table 2: Configurations of membrane systems

Single		**PPy Single System** MB:CA membrane polymerized with PPy
		**PEDOT Single System** MB:CA membrane polymerized with PEDOT
Multi-Layered	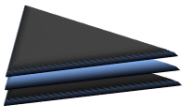	**PPy Multi-Layered System** Two CA membranes polymerized with PPy, with a MB:CA membrane in between
		**PEDOT Multi-Layered System** Two CA membranes polymerized with PEDOT, with a MB:CA membrane in between

2.3 Characterization Methods

To ensure proper functionality of the transdermal patch, it was essential to analyze in detail each component it comprises, verify if its production was carried out properly, and ensure that it is resistant enough for quality and durability during use. To guarantee these properties, the following characterization techniques were conducted.

Morphological Characterization

The surface morphology of fibers and coatings was observed by optical microscopy (OM) using a Leica DMi8 model, and by scanning electron microscopy (SEM) using a Hitachi S2400 model. SEM images were captured using a 20 kV energy beam and prior to image acquisition, the samples were attached to a metal sample holder using a double-sided carbon-based conductive tape (Electron Microscopy Sciences) and then coated with a thin layer of gold-palladium alloy, ensuring a good electron outflow. Additionally, the average diameter of the electrospun fibers was estimated by thirty measurements in each sample using the ImageJ® software.

Chemical Composition Analysis

To evaluate the chemical composition of membranes, by verifying the presence of the compounds added to the membranes, Fourier Transform Infrared Spectroscopy (FTIR) was performed in Attenuated Total Reflectance (ATR) mode using a Thermo Scientific spectrometer (Nicolet Summit X model), acquiring a transmittance spectrum within a wavenumber range from 4000 cm^{-1} to 400 cm^{-1}.

Electrical Conductivity Measurement

The electrical conductivity was obtained by measuring the current–voltage (I–V) values in the different electrospun membranes using a Keithley 6400 Pico-amperemeter/Voltage source, two probe tips, and a computer for recording data. The I–V measurements were repeated three times for three samples, and the average of the slopes was obtained for each membrane. A plot of the current obtained for each applied voltage to a resistive element is directly obtained from the I-V curve. According to Ohm's law, as enunciated in Equation (1):

$$V = R \times I \tag{1}$$

where V is the potential difference (V), R is the resistance (Ω), and I is the current (A), the slope of the I-V curve represents the inverse of the resistance. With this value, the value of the cross-section area and the value of the distance between electrodes, the planar conductivity of each sample was measured on the surface of the membranes using Equation (2):

$$\sigma = \frac{l}{AR} \tag{2}$$

where σ is the electrical conductivity (Scm^{-1}), A is the area of the cross-section of membrane (cm^2), and l is the distance between electrodes (cm). The cross-section was delimited by the electrode length and the thickness of the membrane. A schematic representation of the cross-section area of membranes is illustrated in Figure 28 a) of Appendix D. The thickness of samples was measured with a micrometer in 15 different areas of the membrane, and then calculated the average thickness. The electrodes were painted with a conductive carbon paint (Bare Conductive®) with a 5 mm by 3 mm rectangular shape, 2 mm apart. The probes were placed on the contacts, and the I–V values were acquired. A model of an I-V curve obtained is represented in Figure 28 b) of Appendix D and an example of the calculations conducted for the measurement of planar conductivity of membranes is described in Table 6 of the same Appendix.

Electrochemical Characterization

Cyclic Voltammetry was carried out for membrane systems to evaluate the redox processes and kinetics of electron transfer reactions, using a Gamry Instruments potentiostat (Reference 3000 model). CV measurements were conducted using a two-electrode setup: in this arrangement, the working electrode represents the sample under examination, while the counter electrode is linked to a silver wire positioned 1 cm away, which ensures circuit completion and sustains a consistent interfacial potential. Potentials and currents between the electrodes were then recorded for analysis.

2.4 Drug Release Study

Drug release was performed in a simulated body fluid (SBF) solution, simulating physiological conditions, by containing the same ions as human blood plasma, at nearly equal concentrations. The SBF solution was prepared following the protocol described by Kokubo et al. [50], and its constituents are described in Table 7, in Appendix E. The solution was kept in a refrigerator at 5ºC until use.

To perform drug release tests, each membrane system was immersed in SBF in a fixed volume of 20 mL. The positive electrode of the Voltage-Current source (Keithley 237) was connected to the membrane, 1cm away from the Ag wire (7cm long and 1mm diameter) that was connected to the ground electrode. Different voltage potentials were tested, corresponding to continuous electrical stimuli, and all the tests were performed in a cumulative release of the

drug. Thus, the electrical stimulation was applied for 1 min, then switched off, followed by a 4-minute period of immersion in SBF. Then, a sample of 3 mL was transferred to a quartz cuvette, to perform the absorbance spectra. The extracted sample returned to the vessel, the membrane was again immersed in SBF, and the fixed voltage was then applied again for another period of 1 minute, followed by a 4-minute period of immersion without electrical stimulation. A passive drug release profile was also studied to compare the influence of electrical stimulus with the passive release of drug by diffusion. The UV-Visible spectroscopy was performed after each stimulus, using a JASCO UV-Vis/NIR Spectrophotometer (V-770 model), in the wavelength range of 450 nm to 750 nm, to determine the concentration of MB released using a preliminary calibration curve of MB in SBF. To conduct the drug release study, an absorption-concentration calibration was obtained using the following methodology: a solution of SBF-MB with a concentration of 8.5 mg/L was prepared, followed by sequential dilutions to obtain different concentrations in intervals of 1 mg/L, from 8.5 to 0.5 mg/L. Then, the absorbance spectra for each concentration, shown in Figure 5, was obtained.

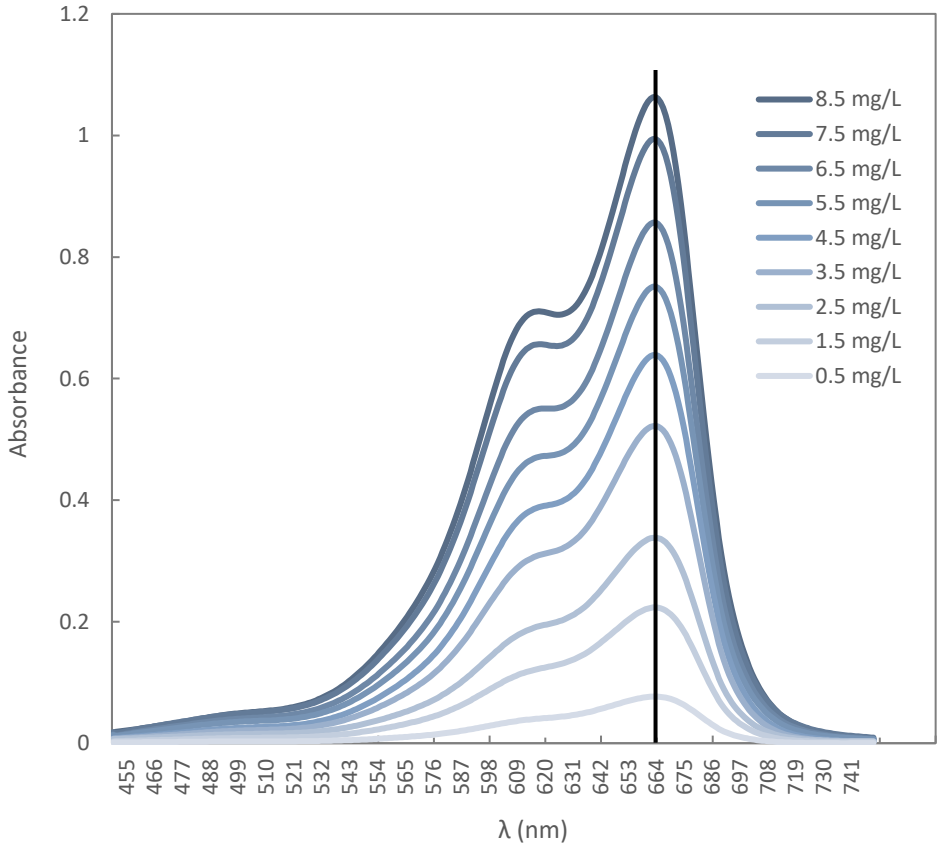

Figure 5: Absorbance spectra for the different concentrations of MB in SBF, used for the calibration curve.

The calibration curve, represented in Figure 6, was estimated by the maximum absorption value of the peak at 664 nm [51].

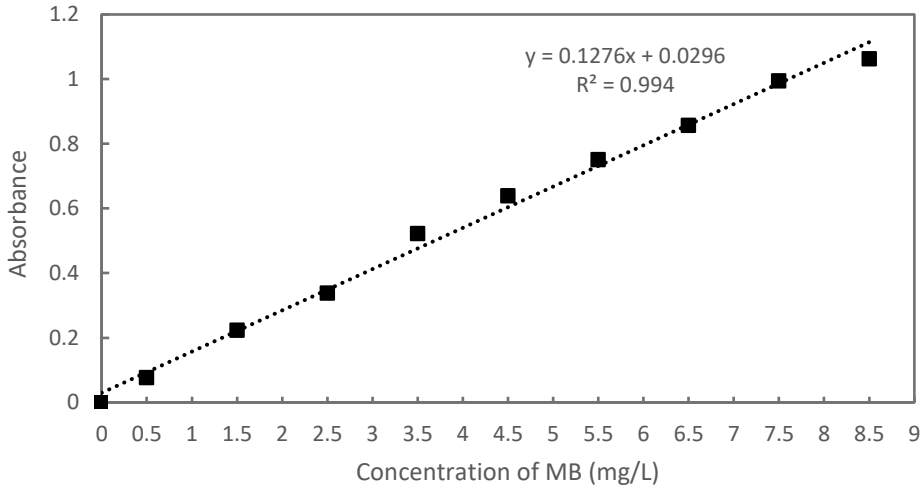

Figure 6: Calibration curve obtained by the maximum absorption value of the peak at 664 nm.

From the calibration curve represented above, was obtained the following empirical correlation, described in Equation (3), between absorption and concentration of MB in SBF:

$$\text{Concentration of MB (664 nm)} \left(\frac{mg}{L}\right) = \frac{\text{Absorbance} - 0.0296}{0.1276} \quad (3)$$

The linear regression of the experimental points obtained shows a good coefficient of determination (R^2 = 0.994). Thus, it was possible to estimate the concentration of MB in passive and active drug release tests in a simulated body fluid solution.

3

RESULTS AND DISCUSSION

3.1 Characterization of MB:CA membranes for Single Systems

3.1.1 MB:CA membranes

Firstly, the morphology of membranes was characterized by optical microscopy. Figure 7 shows a macroscopic (a) and an optical microscopic image (b) of the obtained MB:AC membrane, however, it is not sufficient to evaluate the detailed morphology of the fibers and the distribution of their diameters, even at the highest magnification of the microscope used (200x).

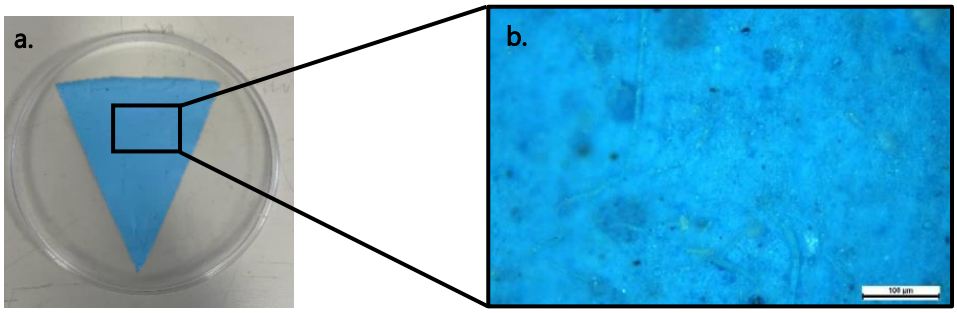

Figure 7: Macroscopic image (a) and optical microscopic image (200x) (b) of the MB:CA membrane.

Furthermore, it becomes difficult to analyze if the deposition of CPs occurred correctly, as shown in Table 8, in Appendix F. In the optical microscopic images of the membranes functionalized with PPy, polymer agglomeration is observed on the surface, yet it is challenging to discern individual fibers within the agglomeration, making it difficult to assess if the PPy uniformly covered them.

In the optical microscopic images of the membranes functionalized with PEDOT, it is not possible at all to observe the deposition of this conductive polymer on the surface of the fibers. Thus, it is necessary to resort to SEM analysis for a more complete and precise analysis. The SEM image of MB:CA fibers, in Figure 8, illustrates the randomness of fiber directions, while the histogram depicting mean fiber diameters shows a relatively uniform distribution, with an average diameter of 224 ± 49 nm.

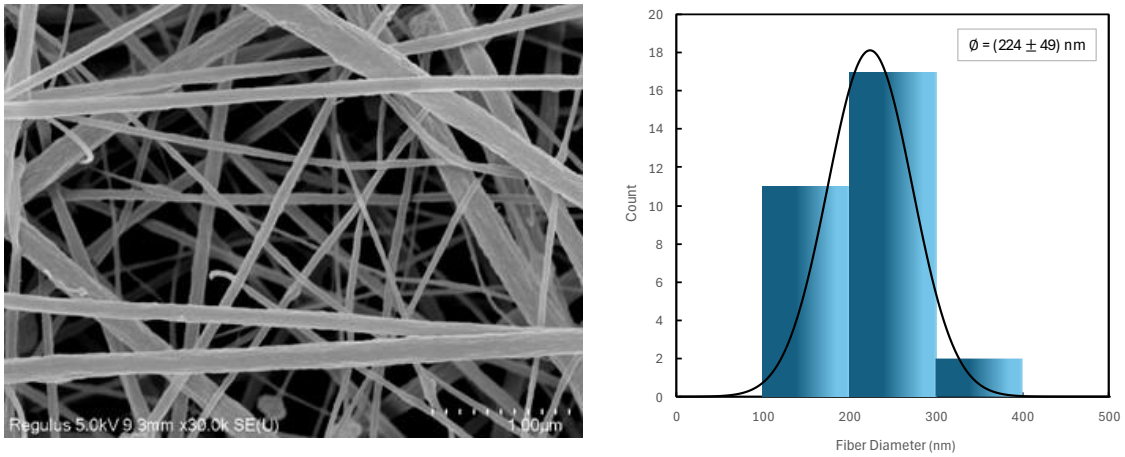

Figure 8: SEM image of MB:CA fibers and respective normal distribution of the mean fiber diameters.

FTIR spectra of the CA membrane, represented in Figure 9, proves the presence of CA in fibers constitution, as the main characteristic peaks of CA were identified at 1040 cm^{-1}, 1231 cm^{-1}, 1369 cm^{-1} and 1742 cm^{-1} due to strain vibrations of the C-O, aryl ether, C-H and C=O groups, respectively [52]. FTIR spectra of the MB:CA membrane, represented in the same figure, was supposed to confirm the presence of MB in fibers, by the characteristic peaks of the model drug at 881 cm^{-1} and 824 cm^{-1} (C–H out of plane bending vibrations of ring), 1055 cm^{-1} (C-S-C vibrations of the heterocycle), 1146 cm^{-1} (C-N bending vibrations), and 1481 cm^{-1} ($C=S^{+}$ stretching vibrations of the heterocycle) [53] [54].

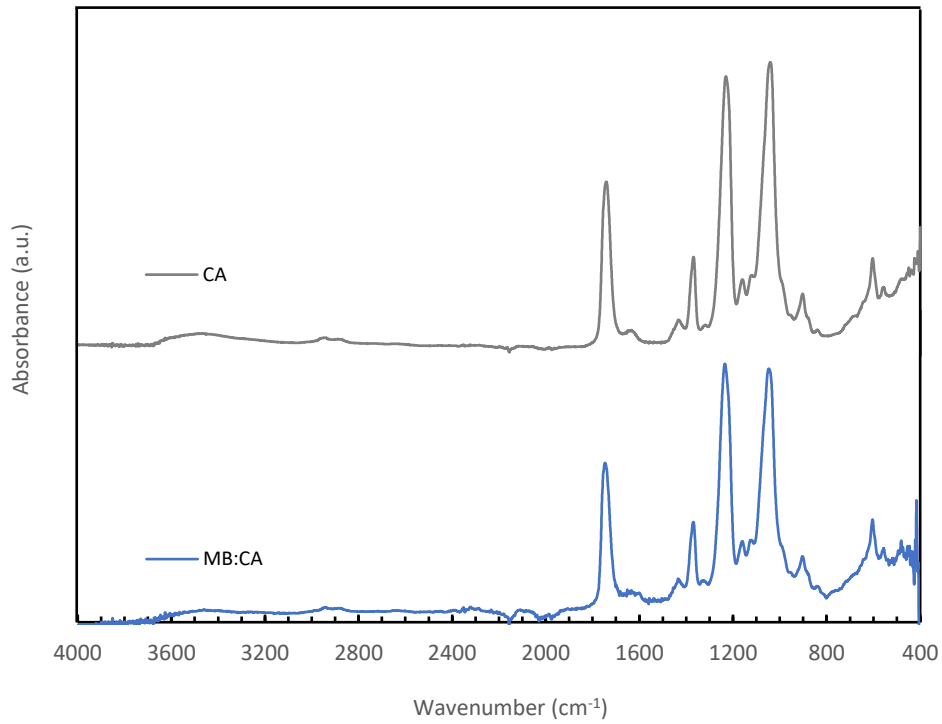

Figure 9: FTIR spectra of CA and MB:CA membranes.

However, by comparing the two spectra, it can be concluded that only the characteristic peaks of CA are visible in the FTIR spectra of MB:CA membrane, given that the amount of drug present in the membranes is significantly reduced (practically residual) in proportion to the amount of CA, so the presence of MB could not be identified in this FTIR spectra.

3.1.2 MB:CA membranes functionalized with PPy

By examining the morphology of CA fibers incorporated with the drug, and functionalized with PPy for 45 minutes, in the SEM image of Figure 10, it becomes evident that they are coated with the CP, whose presence is further confirmed by FTIR analysis. Examination of the histogram reveals a relatively narrow dispersion in terms of fiber diameter, with a mean of 252 ± 41 nm.

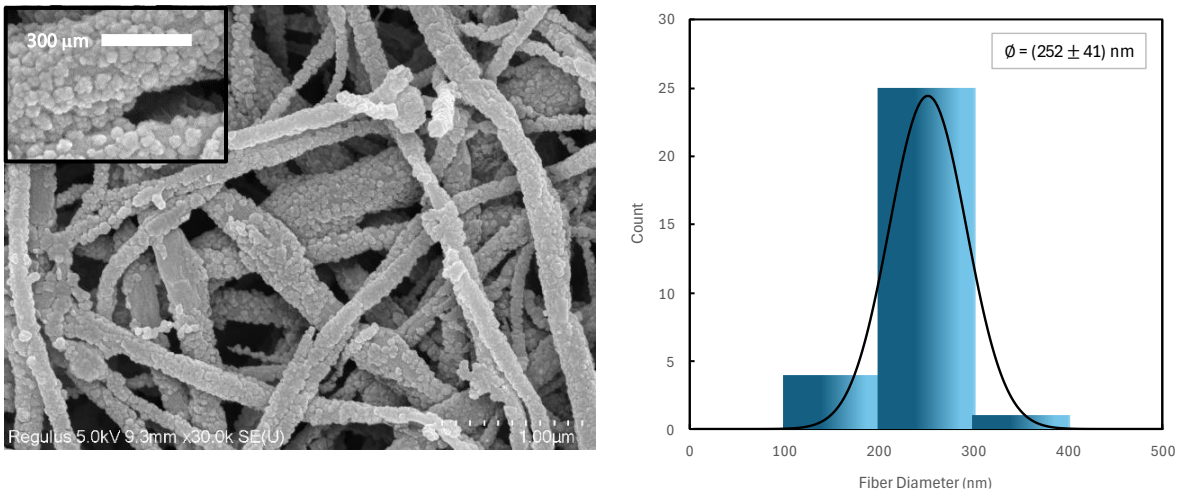

Figure 10: SEM image of PPy_{45}/MB:CA fibers and respective mean fiber diameters.

It is evident that the functionalization of CA fibers with PPy was successful as the characteristic peaks of PPy at 790 cm^{-1}, 965 cm^{-1} and 1548 cm^{-1} were identified in FTIR spectra of PPy/CA membrane, as shown in Figure 11. The first two peaks are attributed to C-H wagging, and the third peak is related to C=C stretching vibration modes [55]. It is possible to conclude that the presence of PPy in PPy/MB:CA membrane is also confirmed through the analysis of FTIR spectra, represented in the same figure, as the characteristic peaks of this CP can be observed at 790 cm^{-1}, 965 cm^{-1} and 1548 cm^{-1} too.

Given that the amount of drug present in the membranes is significantly reduced in proportion to the amount of CA and PPy, MB could not be identified in these membranes too, just as it happened with the MB:CA membranes (Figure 9).

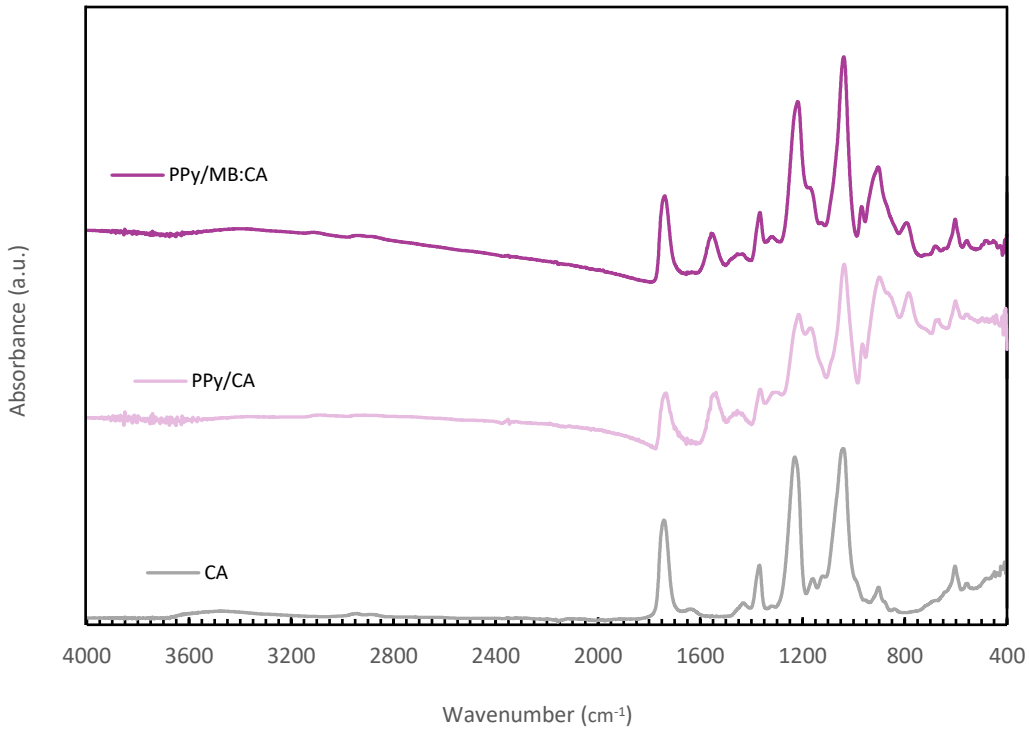

Figure 11: FTIR spectra of PPy/MB:CA, PPy/CA and CA membranes.

3.1.3 MB:CA membranes functionalized with PEDOT

The morphology of CA fibers incorporated with the drug and functionalized with PEDOT was evaluated for three different polymerization times: 45 (Figure 12 a), 90 (Figure 12 b), and 120 (Figure 12 c) minutes. It can be concluded that despite this variation in polymerization time, the membranes do not show significant differences in their morphology, all exhibiting an observable coating of PEDOT and a very close average diameter in the range of 189-201 ± 29-39 nm (201± 29 nm for 45minutes, 189 ± 39 nm for 90 minutes and 190 ± 38 nm for 120 minutes).

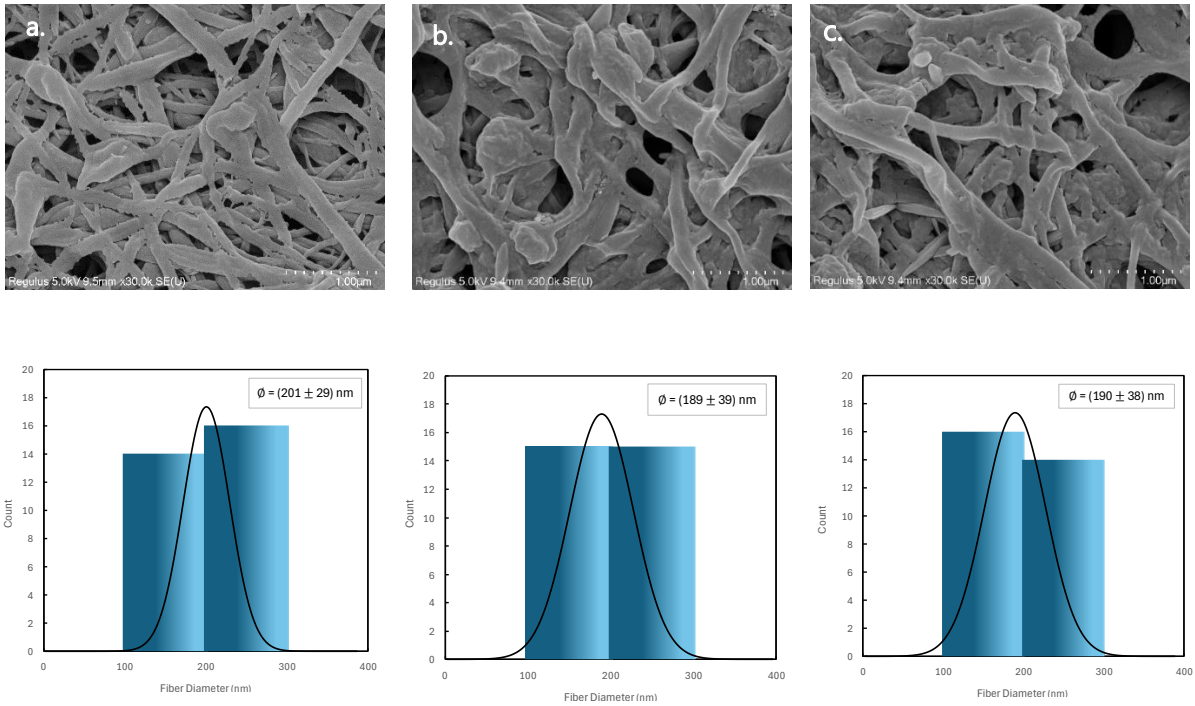

Figure 12: SEM image of PEDOT/MB:CA fibers with a 45-minute (a), 90-minute (b) and 120-minute (c) polymerization time, and respective normal distribution of the mean fiber diameters.

For single systems, a study aimed at evaluating the influence of polymerization time in electrical conductivity in the functionalization of MB:CA membranes, involved the examination of two distinct polymerization times for PPy (45 and 90 minutes), alongside the exploration of three varied polymerization times for PEDOT (45, 90 and 120 minutes). The values of planar conductivity obtained for these membranes are presented in Figure 13, and described in detail in Table 9, in Appendix G.

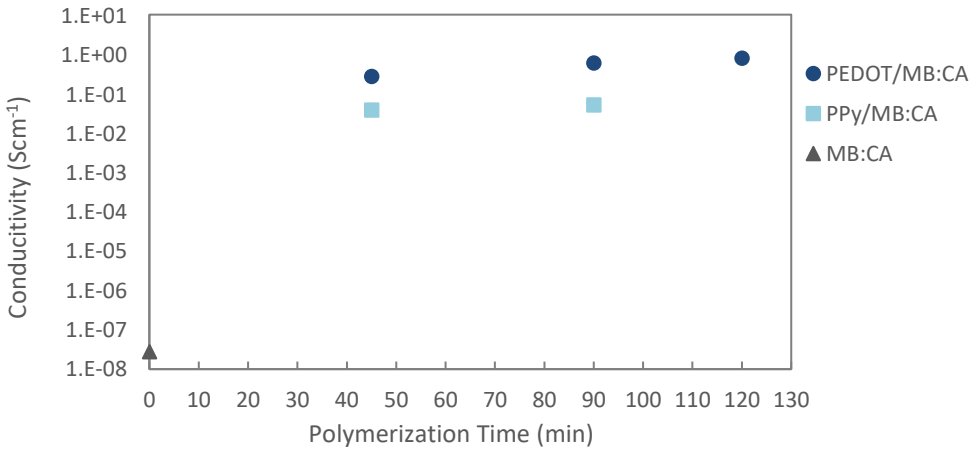

Figure 13: Evaluation of polymerization time in electrical conductivity of functionalized MB:CA membranes.

According to these results, it was decided to project the single systems with:

- MB:CA membrane with a polymerization time of 45 minutes with **PPy** (PPy_{45}/MB:CA), because although the membrane with 90 minutes of polymerization presents a slightly higher conductivity ($5.52 \times 10^{-2} \pm 4.01 \times 10^{-4}$ Scm^{-1}) than the one with 45 minutes ($4.02 \times 10^{-2} \pm 6.99 \times 10^{-5}$ Scm^{-1}), the conductivity values are overall very close and the coverage of CP in fibers was verified by SEM (Figure 10), so by choosing the 45-minute polymerization membrane, it ensures there is less drug loss due to diffusion since the polymerization time under stirring in solution is much shorter;
- MB:CA membrane with a polymerization time of 120 minutes with **PEDOT** ($PEDOT_{120}$/MB:CA), as it presents a higher conductivity value ($8.52 \times 10^{-1} \pm 5.68 \times 10^{-2}$ Scm^{-1}) compared to the membrane with a 45-minute polymerization time ($2.93 \times 10^{-1} \pm 8.82 \times 10^{-2}$ Scm^{-1}) and 90-minute polymerization time ($6.45 \times 10^{-1} \pm 4.51 \times 10^{-2}$ Scm^{-1}).

3.2 Drug Release Tests - PPy and PEDOT Single Systems

The drug release of MB was firstly studied through diffusion for the PPy_{45} Single System (PPy_{45}/MB:CA) and $PEDOT_{120}$ Single System ($PEDOT_{120}$/MB:CA), to be compared with the drug release profile of MB:CA membrane, which had not been functionalized. The drug release profile of the MB:CA membrane through passive release in SBF is shown in Figure 14, indicating a notably rapid release of MB through diffusion.

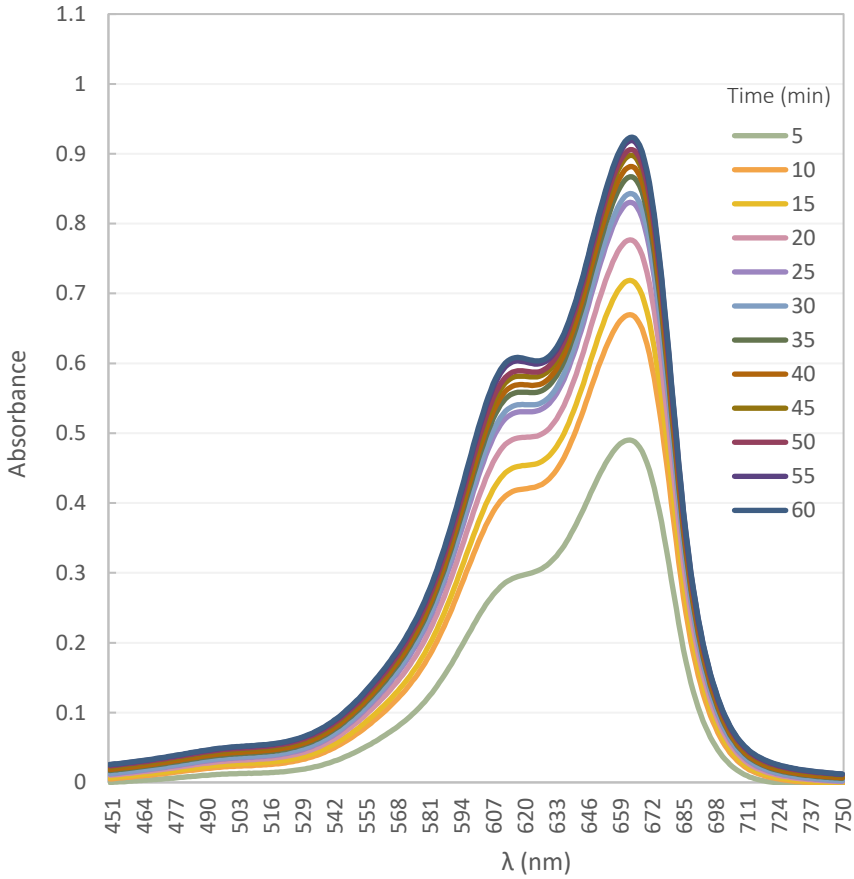

Figure 14: Absorbance spectra of diffusion for the MB:CA membrane in SBF.

As evidenced by the analysis of absorbance spectra of the drug release through diffusion for the single systems constituted by MB:CA membranes functionalized with PPy (Figure 29 of Appendix H) and PEDOT (Figure 30 of Appendix H), no release of MB occurs, as there is no evidence of the absorption of the drug in the spectroscopy analysis at the 664 nm peak in either of the systems. These results can be explained by the instant diffusion of MB in both SBF and water. Since the fiber functionalization processes require the membranes to contact with aqueous solutions, it is possible that the drug was lost through diffusion during the fiber functionalization process. In the case of liquid-phase polymerization of pyrrole, the membranes need to be in magnetic stirring at 100 rpm for 10 minutes in an aqueous solution with pyrrole, followed by a 45-minute constant magnetic stirring period with the addition of the aqueous solution containing the oxidizing agent, resulting in a total contact time with water of 55 minutes. In the case of vapor-phase polymerization of EDOT, although most of the process occurs through vapors, the membranes need to be submerged in magnetic stirring at 100 rpm in the aqueous solution with the oxidizing agent for 20 minutes.

It is expected that the release of MB will be similar in both water and SBF medium where membranes were immersed. Assuming they are identical, it is estimated that within 55 minutes and 20 minutes of release, a significant amount of the model drug will be released. A calibration curve for MB in water medium was obtained (represented in Figure 31, in Appendix I), and it is thus expected that a different medium will not influence the calibration curve. Therefore, it can be predicted that the drug was lost through diffusion, and the active release profiles of MB from the single systems couldn't be evaluated.

Consequently, an alternative system, composed by layered membranes, was tested: its composition relies on an inner MB:CA membrane and two outer CA membranes polymerized with the selected CPs. In this type of structure, the MB:CA membrane never meets water or SBF until subjected to release tests, ensuring that drug loss due to diffusion does not occur until that moment.

3.3 Characterization of membranes for Multi-Layered Systems

3.3.1 CA membranes

In the optical microscopic image of the produced CA membrane, shown in Figure 15 b), it is possible to identify some thin fibers with markedly reduced diameters, although the precise morphology of the fibers is very difficult to analyze. Due to the limitation of magnification through this technique, the fibers were further analyzed by SEM.

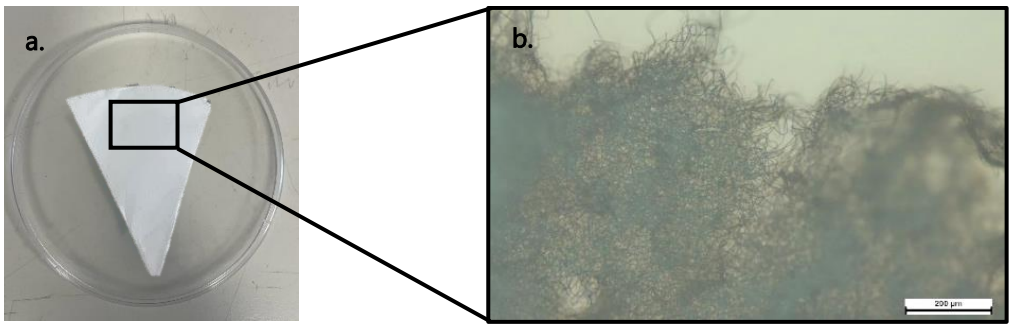

Figure 15: Macroscopic image (a) and optical microscopic image (100x) (b) of the CA membrane.

The SEM image of CA fibers is represented in Figure 16, and comparing the CA to the MB:CA fiber diameters, 340 ± 74 nm and 224 ± 49 nm, respectively, it is possible to conclude that CA fibers in which MB incorporation occurred experience a decrease in their average diameters. This difference can be explained by the increase in the applied voltage during the electrospinning process of MB:CA membranes, as shown in Table 1, and by the decrease of concentration of CA for the polymeric solution with the addition of the drug, as explained in subsection 2.1.1, leading to the formation of fibers with smaller diameters.

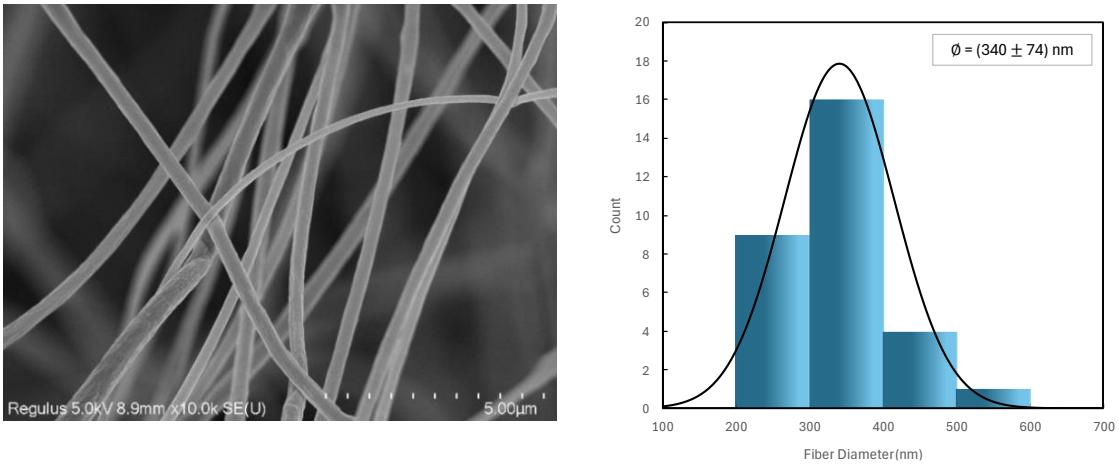

Figure 16: SEM image of CA fibers and respective mean fiber diameters.

3.3.2 CA membranes functionalized with PPy - Outer Layer

A morphological and chemical characterization was performed in CA membranes after a 90-minute polymerization with PPy, through SEM and FTIR (as observed and discussed in Figure 11) to verify if the CP deposited to functionalize the fibers is present in their surface and if uniformly covers them. Figure 17 clearly shows that there is a coverage of PPy along the entire surface of the fibers, with the presence of polymer agglomerations also observed. As observed in the histogram, the fibers present an average diameter of 637 ± 106 nm.

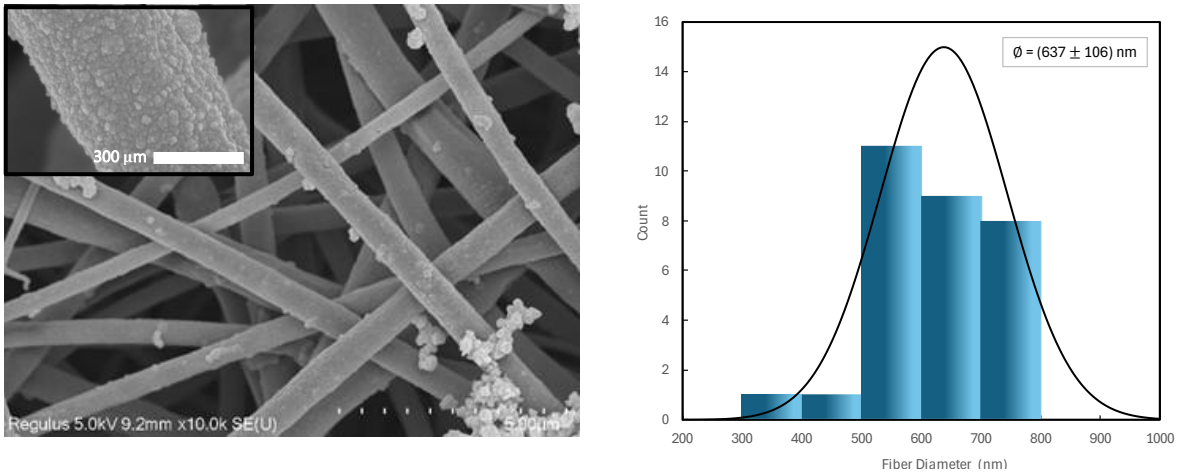

Figure 17: SEM image of PPy/CA fibers and respective mean fiber diameters.

3.3.3 CA membranes functionalized with PEDOT - Outer Layer

The morphological characterization conducted in CA membranes after a 120-minute polymerization with PEDOT, represented in Figure 18, shows numerous randomly distributed fibers, with a uniform coating of PEDOT along the entire surface of the fibers. It can be noted that fewer agglomerations of the CP formed in this polymerization compared to PPy, possibly due to the PEDOT polymerization occurring in the vapor phase, enabling a more homogeneous deposition. The fibers present an average diameter of 609 ± 98 nm, which is similar to the diameter of CA membranes functionalized with PPy. As expected, the diameters of the fibers increase after functionalization, due to the coverage of CPs along the surface of fibers.

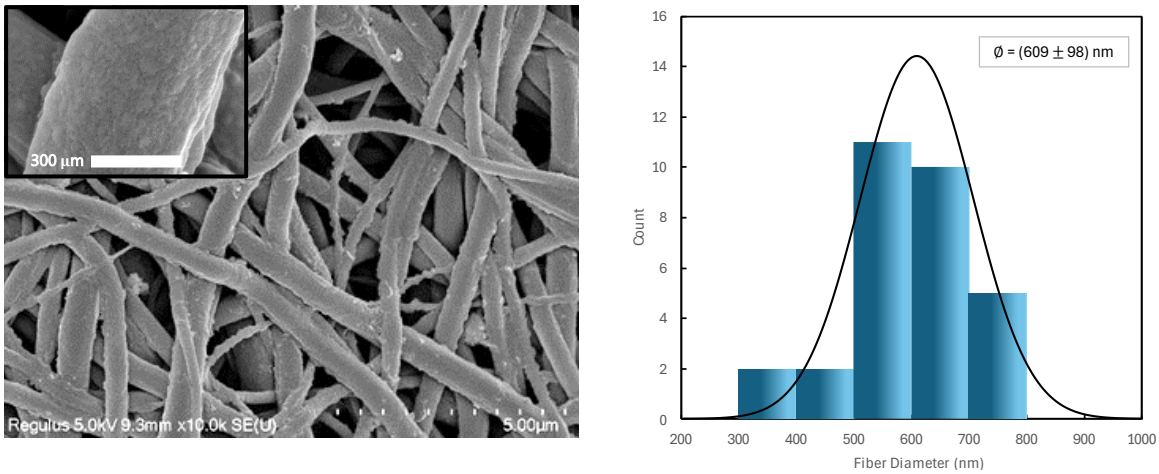

Figure 18: SEM image of PEDOT/CA fibers and respective mean fiber diameters.

FTIR analysis of this membrane was inconclusive, as the characteristic peaks of PEDOT couldn't be identified, as shown in Figure 32, in Appendix J. It was expected to find the characteristic peaks at 1270 cm^{-1}, 1380 cm^{-1}, 1451 cm^{-1}, and 1520 cm^{-1}. These peaks correspond to stretching vibration modes of the C-C bond, stretching of the C-C bond, stretching of the symmetric C=C bond, and stretching of the asymmetric C=C bond, respectively [56] [57].

To assess the electrical conductivity of these membranes coated with the CPs, planar conductivity was measured immediately after their functionalization. The PPy_{90}/CA membrane presented a value of 9.14 x 10^{-2} ± 9.16 x 10^{-4} Scm^{-1}, and the $PEDOT_{120}$/CA membrane presented a value of 8.98 x10^{-2} ± 8.15x10^{-3} Scm^{-1}, which shows an increase compared to the value of 1.05 x 10^{-8} ± 3.26 x 10^{-9} Scm^{-1} for a CA membrane without functionalization. The selection of these polymerization times was based on the study conducted previously by Lago et al. in 2023 [40].

3.4 Drug Release Tests - PPy and PEDOT Multi-Layered Systems

After the production and characterization of membranes for the proposed multi-layered systems, which includes two CA membranes functionalized with CPs for the outer layers and a MB:CA membrane for the inner layer, drug release tests were conducted both passively and actively. Passive release involves diffusion-driven release, serving as a basis for comparison with active release tests involving applied voltage between the electrodes.

In order to obtain information about the oxidation-reduction processes of the CA membrane functionalized with PPy and consequently predict the range of voltages necessary for controlled drug release tests, cyclic voltammetry was performed for this membrane in SBF, as illustrated in Figure 19 a). Three scan rates were studied (25, 100 and 150 mV/s), with five cycles for each, and the third cycle was selected for comparative purposes. It is possible to observe from the graph obtained in Figure 19 b) that at a scan rate of 25 mV/s, more defined oxidation and reduction peaks are observed. It is suggested that the oxidation peak at +0.6 V and the reduction peak at -0.5 V are caused by the redox reactions of PPy that occur at the cathode (working electrode) of the respective system.

The oxidation reaction of PPy associated with the observed peaks is:

$PPy^0 \rightarrow PPy^+ + e^-$

And the reduction reaction is:

$PPy^+ + e^- \rightarrow PPy^0$

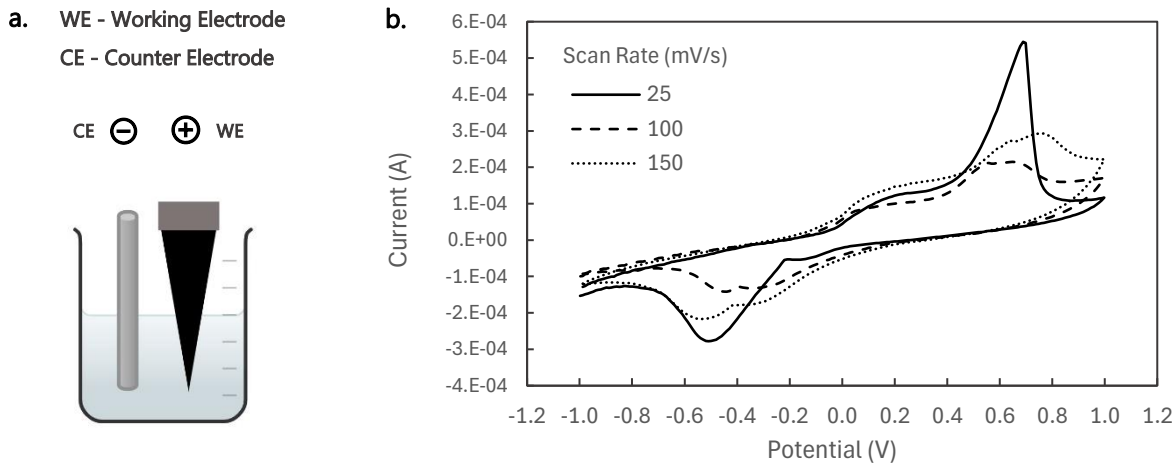

Figure 19: Schematic diagram of cyclic voltammetry (a) and the third cycle of the cyclic voltammogram obtained for the PPy/CA membrane (b).

Therefore, positive, and negative voltage values were applied to the system, along with diffusion for the controlled drug release tests, corresponding to voltages above and below which the anodic and cathodic peaks occur. For the negative voltages, potentials of -0.3 V and -0.8 V were applied, and for the positive voltages, potentials of +0.3 V, +0.8 V were applied. The drug release profile of the PPy_{90} Multi-Layered System that was obtained is illustrated in Figure 20. In order to obtain a comparative study of the multi-layered systems functionalized with the two different conductive polymers, the same potentials were applied to the $PEDOT_{120}$ Multi-Layered System, and its drug release profile that was obtained is shown in Figure 21.

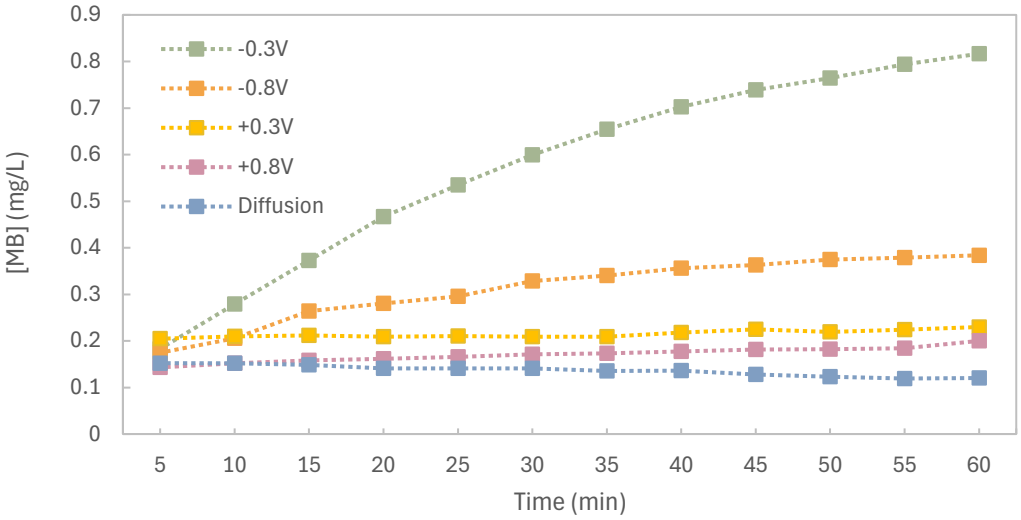

Figure 20: Drug release profile of MB for PPy multi-layered system.

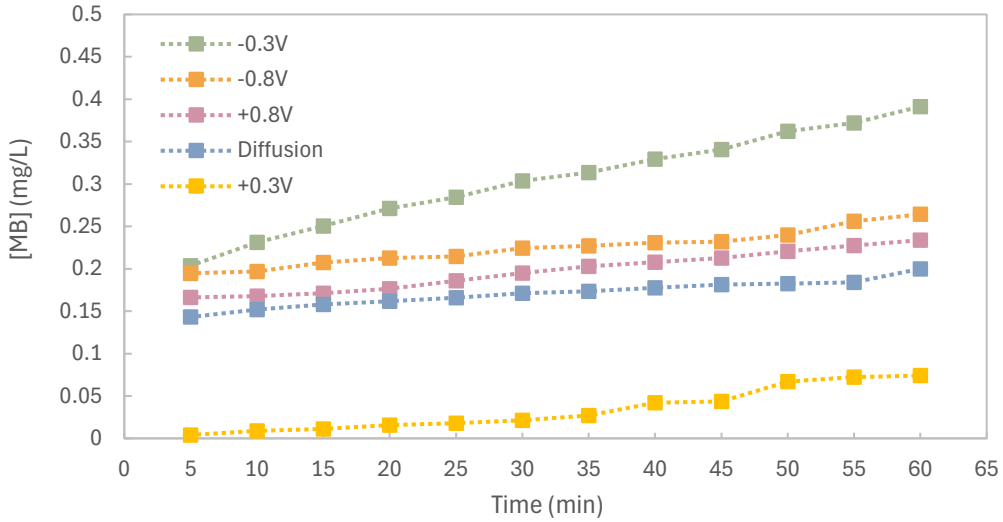

Figure 21: Drug release profile of MB for PEDOT multi-layered system.

By measuring the concentrations of MB achieved after 60 minutes of release, the amount of the model drug present in 20 mL of SBF was quantified, and the percentage of the drug released was calculated relative to an initial amount of 300 µg of MB in each membrane. These results are shown in Table 10 in Appendix K, and through the analysis of the release profile of multi-layered systems, it is possible to conclude that the most pronounced drug release occurs in both systems when a voltage of -0.3V is applied, with this release being more pronounced for the system functionalized with PPy. It is also possible to conclude that both systems exhibit higher MB release when negative voltages are applied compared to the positive ones, possibly due to the positively charged nature of the drug.

Comparing the release profiles of these systems with those studied previously by Lago et al. [40] with the selection of a negatively charged drug (IBU), the following can be observed: in both PEDOT and PPy multi-layered systems, the applied voltage resulting in superior retention of IBU was -0.3V, and the applied voltages resulting in greater release of this drug were +0.5V and +0.3V. Therefore, it is concluded that these systems have practically an opposite release profile to the systems studied in this thesis. Given that the conductive polymers used were the same, and that the membrane functionalization processes of CA fibers were replicated with the same CPs, these values are possibly related to the charge of the drug used for the electrically controlled drug release systems. Conductive polymers can bind to and detach from different drugs due to their redox reactions by electrical stimulation. Thus, the conductive polymer can induce the retention or the release of drug molecules into the surrounding medium depending on the applied potential.

The morphology of functionalized membranes was evaluated after the drug release upon an applied voltage of -0.3V, since it is the one that presents a higher release of MB through the fibers. The SEM images are represented below for PPy_{90}/CA membranes (Figure 22) and for $PEDOT_{120}$/CA membranes (Figure 23).

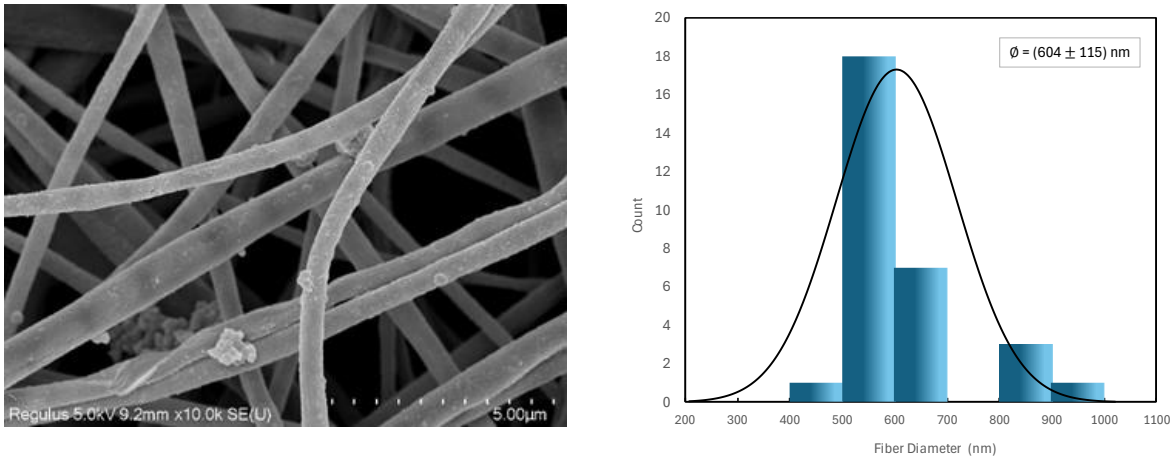

Figure 22: SEM image of PPy/CA fibers after drug release and respective mean fiber diameters.

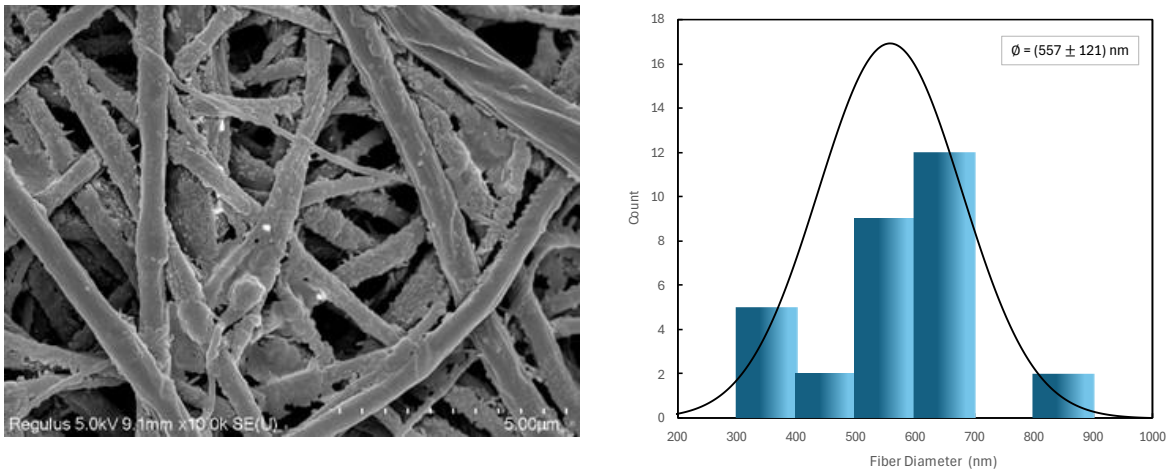

Figure 23: SEM image of PEDOT/CA fibers after drug release and respective mean fiber diameters.

It can be observed that after the release tests, the fibers remain coated with a layer of PPy and PEDOT. The membranes polymerized with PPy and PEDOT do not show a significant reduction in the average fiber diameter after the drug release test. Although the average value is slightly lower, the standard deviation is superior in the fibers after release, so it cannot be directly related to the release process. Initially, PPy/CA fibers had a mean diameter of 637 ± 106 nm, while a mean diameter of 604 ± 115 nm was obtained after the drug release test. PEDOT/CA fibers had a mean diameter of 609 ± 98 nm, before the drug release, while a mean diameter of 557±121 nm was obtained after the drug release test. Thus, it can be concluded that the controlled drug release tests were not destructive to the morphology of the fibers or the coating of the CPs, despite the release of MB occurring through the fibers.

The planar conductivity of the functionalized membranes of multi-layered systems was measured before and after drug release tests and those values are presented in Table 3. The electrical conductivity values obtained after the drug release test relate to the application of an electrical stimulus of -0.3 V for one hour in SBF. A slight decrease in conductivity values is observed, which may be explained by a possible loss of adhesion of the CP to the surface of the fibers during the drug release tests.

Table 3: Planar conductivity of functionalized CA membranes before and after the drug release.

Conductive Membranes	Planar Conductivity (Scm^{-1})	
	Before Drug Release	After Drug Release
PPy_{90}/CA	$9.14 \times 10^{-2} \pm 9.16 \times 10^{-4}$	$8.24 \times 10^{-3} \pm 7.67 \times 10^{-4}$
$PEDOT_{120}$/CA	$8.98 \times 10^{-2} \pm 8.15 \times 10^{-3}$	$8.01 \times 10^{-3} \pm 7.77 \times 10^{-4}$

To assess the evolution of conductivity over time, electrical conductivity was measured for the four proposed systems immediately after their functionalization and after four months. These values are presented in Table 4.

Table 4: Evaluation of planar conductivity of the membranes over time.

Type of system	Conductive membranes	Planar Conductivity (Scm^{-1})	
		After functionalization	After four months
Single	PPy_{45}/MB:CA	$4.02 \times 10^{-2} \pm 6.99 \times 10^{-5}$	$8.78 \times 10^{-3} \pm 2.47 \times 10^{-7}$
	$PEDOT_{120}$/MB:CA	$8.25 \times 10^{-1} \pm 5.68 \times 10^{-2}$	$1.06 \times 10^{-2} \pm 1.02 \times 10^{-3}$
Multi-Layered	PPy_{90}/CA	$9.14 \times 10^{-2} \pm 9.16 \times 10^{-4}$	$2.11 \times 10^{-2} \pm 3.00 \times 10^{-6}$
	$PEDOT_{120}$/CA	$8.98 \times 10^{-2} \pm 8.15 \times 10^{-3}$	$2.81 \times 10^{-2} \pm 1.77 \times 10^{-3}$

It can be concluded that over the course of four months, there is a slight decrease in electrical conductivity in all membranes. As the membranes are coated with PPy and PEDOT, this decrease could be related to polymer oxidation, as the membranes, after functionalization, are left to dry at room temperature and therefore met the surrounding air [58] [59]. The conductivity of the membranes functionalized with PEDOT presents similar values to PPy, around 10^{-1} / 10^{-2} (Scm^{-1}) shortly after production and around 10^{-2} /10^{-3} (Scm^{-1}) after four months.

4

CONCLUSIONS AND FUTURE PERSPECTIVES

Presently, with the advancement of various stimulus-responsive materials and technologies, it is possible to regulate drug release through diverse stimuli. To investigate the drug release behavior under electrical stimuli, two types of systems comprised of cellulose acetate polymeric membranes were developed in this study using the electrospinning process. Single systems consisting of a single CA membrane with the model drug, functionalized with two conductive polymers, PPy and PEDOT, were produced. Additionally, multi-layered systems were also produced, comprising an inner layer of CA membrane with MB and two outer layers of CA functionalized with PPy and PEDOT. Following electrospinning, all membranes were divided into equal triangular pieces to ensure uniform interior and exterior membrane sections due to radial thickness variation. For the polymerization of CA membranes with PPy and PEDOT, optimized protocols from prior works were employed. For CA membranes incorporated with MB, the influence of different polymerization times for PPy and PEDOT was studied, and in the case of vapor phase polymerization of EDOT, the MB:CA membrane polymerization protocol had to be adapted to obtain non-brittle membranes.

Optical microscopy did not provide the desired precision in observing the morphology and diameter distribution of the produced fibers. Therefore, morphology analysis was conducted using SEM, which revealed uniformly coated conducting polymer layers on fibers functionalized with PPy and PEDOT, both with and without the drug. The presence of PPy in CA and MB:CA membranes was confirmed by FTIR, although PEDOT presence was not identified in this analysis.

The highest planar electrical conductivity values were observed for MB:CA membranes functionalized with PEDOT for a duration of 120 minutes. Regarding PPy, the highest electrical conductivity values were observed for CA membranes, without the drug, functionalized for 90

minutes. Overall, all membranes exhibited high electrical conductivity values in the range of 10^{-1} and 10^{-2} Scm^{-1}.

The study on the effect of applied voltage between membrane systems and the silver electrode for drug release profile evaluation was inconclusive for single systems, possibly due to drug loss by diffusion during the functionalization processes. In future studies, to overcome this limitation and to study drug release under electrical stimuli, the production of these membranes through coaxial electrospinning could be tested. If these systems consist of an inner layer of the drug and are surrounded by an outer layer of CA, diffusion can be delayed, as reported in previous studies [60]. For the effect of applied voltage on drug release profile evaluation for multi-layered systems, it was observed that for both systems, rapid drug release occurred under negative voltages (maximum at -0.3V), and delayed drug release compared to diffusion was observed under positive voltages. Compared to previous studies, it can be concluded that drug release in electrically controlled systems is influenced by the applied electrical stimulus and the charge of the selected drug molecule. Considering the considerably reduced concentration of released drug (maximum value near 1mg/L), future studies could consider increasing the amount of drug added. To study an ON/OFF type drug release profile, further studies should consider modeling based on the voltages at which the highest drug release (-0.3V) and retention (+0.3V and +0.8V) were observed.

After active drug release tests of multi-layered systems, morphological characterization by SEM was conducted on the membranes. It was concluded that the fibers remained coated with conductive polymers, proving that their integrity was maintained even after undergoing release tests. Electrical conductivity measurements after the tests revealed a slight decrease but confirming that the membranes remained electrically conductive.

This study has demonstrated the feasibility of obtaining a controlled drug release profile through the developed membrane systems. These results are promising as they pave the way for the exploration of automatic electronic control systems and periodic controlled dosing in the future, with an increased understanding of the factors directly influencing their release and control. However, in future studies, it is essential to verify the results by conducting more tests to obtain better statistical significance for each assay and to simulate these release tests using a prototype of a transdermal patch, to simulate real drug release conditions more accurately.

5 REFERENCES

[1] D. Bird and N. M. Ravindra, "Transdermal drug delivery and patches—An overview," *Med Devices Sens*, vol. 3, no. 6, Dec. 2020, doi: 10.1002/mds3.10069.

[2] S. Adepu and S. Ramakrishna, "Controlled Drug Delivery Systems: Current Status and Future Directions," *Molecules*, vol. 26, no. 19, p. 5905, Sep. 2021, doi: 10.3390/molecules26195905.

[3] A. C. Baptista, M. Brito, A. Marques, and I. Ferreira, "Electronic control of drug release from gauze or cellulose acetate fibres for dermal applications," *J Mater Chem B*, vol. 9, no. 16, pp. 3515–3522, 2021, doi: 10.1039/D1TB00249J.

[4] S. Merino, C. Martín, K. Kostarelos, M. Prato, and E. Vázquez, "Nanocomposite Hydrogels: 3D Polymer–Nanoparticle Synergies for On-Demand Drug Delivery," *ACS Nano*, vol. 9, no. 5, pp. 4686–4697, May 2015, doi: 10.1021/acsnano.5b01433.

[5] M. Rostamitabar, A. M. Abdelgawad, S. Jockenhoevel, and S. Ghazanfari, "Drug-Eluting Medical Textiles: From Fiber Production and Textile Fabrication to Drug Loading and Delivery," *Macromol Biosci*, vol. 21, no. 7, p. 2100021, Jul. 2021, doi: 10.1002/mabi.202100021.

[6] E. Kotroni *et al.*, "In Vivo Evaluation of the Anti-Inflammatory Activity of Electrospun Micro/Nanofibrous Patches Loaded with Pinus halepensis Bark Extract on Hairless Mice Skin," *Materials*, vol. 12, no. 16, p. 2596, Aug. 2019, doi: 10.3390/ma12162596.

[7] M. Gouda, A. Hebeish, and A. Aljafari, "Synthesis and characterization of novel drug delivery system based on cellulose acetate electrospun nanofiber mats," *Journal of Industrial Textiles*, vol. 43, no. 3, pp. 319–329, Jan. 2014, doi: 10.1177/1528083713495250.

[8] P. Taepaiboon, U. Rungsardthong, and P. Supaphol, "Vitamin-loaded electrospun cellulose acetate nanofiber mats as transdermal and dermal therapeutic agents of vitamin A

acid and vitamin E," *European Journal of Pharmaceutics and Biopharmaceutics*, vol. 67, no. 2, pp. 387–397, Sep. 2007, doi: 10.1016/j.ejpb.2007.03.018.

[9] X. Zhao, L. Yildirimer, Z. Y. (William) Lin, and W. Cui, "Bionanofibers in drug delivery * *Xin Zhao and Lara Yildirimer contributed equally.," in *Nanobiomaterials in Drug Delivery*, Elsevier, 2016, pp. 403–445. doi: 10.1016/B978-0-323-42866-8.00012-5.

[10] V. Salles *et al.*, "Synthesis and Characterization of Advanced Carbon-Based Nanowires – Study of Composites Actuation Capabilities Containing These Nanowires as Fillers," in *Nanowires - Recent Advances*, InTech, 2012. doi: 10.5772/54384.

[11] R. Jain, S. Shetty, and K. S. Yadav, "Unfolding the electrospinning potential of biopolymers for preparation of nanofibers," *J Drug Deliv Sci Technol*, vol. 57, p. 101604, Jun. 2020, doi: 10.1016/j.jddst.2020.101604.

[12] M. A. Wsoo, S. Shahir, S. P. Mohd Bohari, N. H. M. Nayan, and S. I. A. Razak, "A review on the properties of electrospun cellulose acetate and its application in drug delivery systems: A new perspective," *Carbohydr Res*, vol. 491, p. 107978, May 2020, doi: 10.1016/j.carres.2020.107978.

[13] K. Khoshnevisan *et al.*, "Cellulose acetate electrospun nanofibers for drug delivery systems: Applications and recent advances," *Carbohydr Polym*, vol. 198, pp. 131–141, Oct. 2018, doi: 10.1016/j.carbpol.2018.06.072.

[14] A. W. Jatoi, I. S. Kim, and Q.-Q. Ni, "Cellulose acetate nanofibers embedded with AgNPs anchored TiO2 nanoparticles for long term excellent antibacterial applications," *Carbohydr Polym*, vol. 207, pp. 640–649, Mar. 2019, doi: 10.1016/j.carbpol.2018.12.029.

[15] M. Q. Khan *et al.*, "Fabrication of antibacterial electrospun cellulose acetate/ silver-sulfadiazine nanofibers composites for wound dressings applications," *Polym Test*, vol. 74, pp. 39–44, Apr. 2019, doi: 10.1016/j.polymertesting.2018.12.015.

[16] W. Liang *et al.*, "Synthesis of cellulose diacetate based copolymer electrospun nanofibers for tissues scaffold," *Appl Surf Sci*, vol. 443, pp. 374–381, Jun. 2018, doi: 10.1016/j.apsusc.2018.02.087.

[17] L. Xu, Y. Yang, Y. Mao, and Z. Li, "Self-Powerbility in Electrical Stimulation Drug Delivery System," *Adv Mater Technol*, vol. 7, no. 2, Feb. 2022, doi: 10.1002/admt.202100055.

[18] A. Gandhi, A. Paul, S. O. Sen, and K. K. Sen, "Studies on thermoresponsive polymers: Phase behaviour, drug delivery and biomedical applications," *Asian J Pharm Sci*, vol. 10, no. 2, pp. 99–107, Apr. 2015, doi: 10.1016/j.ajps.2014.08.010.

[19] V. Sharma and A. Sundaramurthy, "Multilayer capsules made of weak polyelectrolytes: a review on the preparation, functionalization and applications in drug delivery," *Beilstein Journal of Nanotechnology*, vol. 11, pp. 508–532, Mar. 2020, doi: 10.3762/bjnano.11.41.

[20] A. Servant, L. Methven, R. P. Williams, and K. Kostarelos, "Electroresponsive Polymer–Carbon Nanotube Hydrogel Hybrids for Pulsatile Drug Delivery In Vivo," *Adv Healthc Mater*, vol. 2, no. 6, pp. 806–811, Jun. 2013, doi: 10.1002/adhm.201200193.

[21] C. Liu *et al.*, "A NIR-controlled cage mimicking system for hydrophobic drug mediated cancer therapy," *Biomaterials*, vol. 139, pp. 151–162, Sep. 2017, doi: 10.1016/j.biomaterials.2017.06.008.

[22] J. Qu, X. Zhao, P. X. Ma, and B. Guo, "Injectable antibacterial conductive hydrogels with dual response to an electric field and pH for localized 'smart' drug release," *Acta Biomater*, vol. 72, pp. 55–69, May 2018, doi: 10.1016/j.actbio.2018.03.018.

[23] M. E. Alkahtani *et al.*, "Electroactive Polymers for On-Demand Drug Release," *Adv Healthc Mater*, vol. 13, no. 3, Jan. 2024, doi: 10.1002/adhm.202301759.

[24] D. Samanta, R. Mehrotra, K. Margulis, and R. N. Zare, "On-demand electrically controlled drug release from resorbable nanocomposite films," *Nanoscale*, vol. 9, no. 42, pp. 16429–16436, 2017, doi: 10.1039/C7NR06443H.

[25] H. Palza, P. Zapata, and C. Angulo-Pineda, "Electroactive Smart Polymers for Biomedical Applications," *Materials*, vol. 12, no. 2, p. 277, Jan. 2019, doi: 10.3390/ma12020277.

[26] B. Maharjan *et al.*, "In-situ polymerized polypyrrole nanoparticles immobilized poly(ε-caprolactone) electrospun conductive scaffolds for bone tissue engineering," *Materials Science and Engineering: C*, vol. 114, p. 111056, Sep. 2020, doi: 10.1016/j.msec.2020.111056.

[27] Y. Zhao, Y. Liang, S. Ding, K. Zhang, H. Mao, and Y. Yang, "Application of conductive PPy/SF composite scaffold and electrical stimulation for neural tissue engineering," *Biomaterials*, vol. 255, p. 120164, Oct. 2020, doi: 10.1016/j.biomaterials.2020.120164.

[28] Y. Liu, A. P. F. Turner, M. Zhao, and W. C. Mak, "Processable enzyme-hybrid conductive polymer composites for electrochemical biosensing," *Biosens Bioelectron*, vol. 100, pp. 374–381, Feb. 2018, doi: 10.1016/j.bios.2017.09.021.

[29] Y. Park, J. Jung, and M. Chang, "Research Progress on Conducting Polymer-Based Biomedical Applications," *Applied Sciences*, vol. 9, no. 6, p. 1070, Mar. 2019, doi: 10.3390/app9061070.

[30] D. S. W. Gunasekara, X. Niu, W. Lqbal, Y. He, and H. Liu, "Pyrrole Coating with In Situ Polymerization for Piezoresistive Sensor Development - A Review," *Macromol Res*, vol. 30, no. 3, pp. 153–162, Mar. 2022, doi: 10.1007/s13233-022-0022-z.

[31] S. Nie, Z. Li, Y. Yao, and Y. Jin, "Progress in Synthesis of Conductive Polymer Poly(3,4-Ethylenedioxythiophene)," *Front Chem*, vol. 9, Dec. 2021, doi: 10.3389/fchem.2021.803509.

[32] M. R. Abidian, D. -H. Kim, and D. C. Martin, "Conducting-Polymer Nanotubes for Controlled Drug Release," *Advanced Materials*, vol. 18, no. 4, pp. 405–409, Feb. 2006, doi: 10.1002/adma.200501726.

[33] D. Müller, C. R. Rambo, D.O.S.Recouvreux, L. M. Porto, and G. M. O. Barra, "Chemical in situ polymerization of polypyrrole on bacterial cellulose nanofibers," *Synth Met*, vol. 161, no. 1–2, pp. 106–111, Jan. 2011, doi: 10.1016/j.synthmet.2010.11.005.

[34] D. Esrafilzadeh, J. M. Razal, S. E. Moulton, E. M. Stewart, and G. G. Wallace, "Multifunctional conducting fibres with electrically controlled release of ciprofloxacin," *Journal of Controlled Release*, vol. 169, no. 3, pp. 313–320, Aug. 2013, doi: 10.1016/j.jconrel.2013.01.022.

[35] L. Tang, J. Han, Z. Jiang, S. Chen, and H. Wang, "Flexible conductive polypyrrole nanocomposite membranes based on bacterial cellulose with amphiphobicity," *Carbohydr Polym*, vol. 117, pp. 230–235, Mar. 2015, doi: 10.1016/j.carbpol.2014.09.049.

[36] R. Wadhwa, C. F. Lagenaur, and X. T. Cui, "Electrochemically controlled release of dexamethasone from conducting polymer polypyrrole coated electrode," *Journal of Controlled Release*, vol. 110, no. 3, pp. 531–541, Feb. 2006, doi: 10.1016/j.jconrel.2005.10.027.

[37] K. Krukiewicz and J. K. Zak, "Conjugated polymers as robust carriers for controlled delivery of anti-inflammatory drugs," *J Mater Sci*, vol. 49, no. 16, pp. 5738–5745, Aug. 2014, doi: 10.1007/s10853-014-8292-2.

[38] C. Boehler, F. Oberueber, and M. Asplund, "Tuning drug delivery from conducting polymer films for accurately controlled release of charged molecules," *Journal of Controlled Release*, vol. 304, pp. 173–180, Jun. 2019, doi: 10.1016/j.jconrel.2019.05.017.

[39] D. Svirskis, J. Travas-Sejdic, A. Rodgers, and S. Garg, "Electrochemically controlled drug delivery based on intrinsically conducting polymers," *Journal of Controlled Release*, vol. 146, no. 1, pp. 6–15, Aug. 2010, doi: 10.1016/j.jconrel.2010.03.023.

[40] B. Lago, M. Brito, C. M. M. Almeida, I. Ferreira, and A. C. Baptista, "Functionalisation of Electrospun Cellulose Acetate Membranes with PEDOT and PPy for Electronic Controlled

Drug Release," *Nanomaterials*, vol. 13, no. 9, p. 1493, Apr. 2023, doi: 10.3390/nano13091493.

[41] C. Ding, S. Xu, J. Wang, Y. Liu, P. Chen, and S. Feng, "Controlled loading and release of methylene blue in layer-by-layer assembled polyelectrolyte films," *Materials Science and Engineering: C*, vol. 32, no. 4, pp. 670–673, May 2012, doi: 10.1016/j.msec.2012.01.005.

[42] Y. Gao, K. Y. Wong, A. Ahiabu, and M. J. Serpe, "Sequential and controlled release of small molecules from poly(N-isopropylacrylamide) microgel-based reservoir devices," *J Mater Chem B*, vol. 4, no. 30, pp. 5144–5150, 2016, doi: 10.1039/C6TB00864J.

[43] T. M. Elmorsi, "Equilibrium Isotherms and Kinetic Studies of Removal of Methylene Blue Dye by Adsorption onto Miswak Leaves as a Natural Adsorbent," *J Environ Prot (Irvine, Calif)*, vol. 02, no. 06, pp. 817–827, 2011, doi: 10.4236/jep.2011.26093.

[44] Y. Talbi, D. Brulin, E. Campo, and J.-Y. Fourniols, "Controlled Permeation of Lidocaine Hydrochloride Using a Smart Drug Delivery System," in *Biomedical Engineering*, Calgary,AB,Canada: ACTAPRESS, 2017. doi: 10.2316/P.2017.852-024.

[45] Y. Yang *et al.*, "Self-Powered Controllable Transdermal Drug Delivery System," *Adv Funct Mater*, vol. 31, no. 36, p. 2104092, Sep. 2021, doi: 10.1002/adfm.202104092.

[46] R. Vadlapatla, E. Y. Wong, and S. G. Gayakwad, "Electronic drug delivery systems: An overview," *J Drug Deliv Sci Technol*, vol. 41, pp. 359–366, Oct. 2017, doi: 10.1016/j.jddst.2017.08.008.

[47] A. Salimi and A. Roosta, "Experimental solubility and thermodynamic aspects of methylene blue in different solvents," *Thermochim Acta*, vol. 675, pp. 134–139, May 2019, doi: 10.1016/j.tca.2019.03.024.

[48] A. C. Baptista *et al.*, "Cellulose-based electrospun fibers functionalized with polypyrrole and polyaniline for fully organic batteries," *J Mater Chem A Mater*, vol. 6, no. 1, pp. 256–265, 2018, doi: 10.1039/C7TA06457H.

[49] R. Brooke, P. Cottis, P. Talemi, M. Fabretto, P. Murphy, and D. Evans, "Recent advances in the synthesis of conducting polymers from the vapour phase," *Prog Mater Sci*, vol. 86, pp. 127–146, May 2017, doi: 10.1016/j.pmatsci.2017.01.004.

[50] T. Kokubo and H. Takadama, "How useful is SBF in predicting in vivo bone bioactivity?," *Biomaterials*, vol. 27, no. 15, pp. 2907–2915, May 2006, doi: 10.1016/j.biomaterials.2006.01.017.

[51] V.-P. Dinh *et al.*, "Insight into the adsorption mechanisms of methylene blue and chromium(III) from aqueous solution onto pomelo fruit peel," *RSC Adv*, vol. 9, no. 44, pp. 25847–25860, 2019, doi: 10.1039/C9RA04296B.

[52] R. O. Asriza, Ropalia, D. Humaira, G. O. Ryaldi, and Zomi, "Characterization of cellulose acetate functional groups synthesized from corn husk (Zea mays)," *IOP Conf Ser Earth Environ Sci*, vol. 926, no. 1, p. 012060, Nov. 2021, doi: 10.1088/1755-1315/926/1/012060.

[53] O. V. Ovchinnikov, A. V. Evtukhova, T. S. Kondratenko, M. S. Smirnov, V. Yu. Khokhlov, and O. V. Erina, "Manifestation of intermolecular interactions in FTIR spectra of methylene blue molecules," *Vib Spectrosc*, vol. 86, pp. 181–189, Sep. 2016, doi: 10.1016/j.vibspec.2016.06.016.

[54] A. A. Alshehri and M. A. Malik, "Biogenic fabrication of ZnO nanoparticles using Trigonella foenum-graecum (Fenugreek) for proficient photocatalytic degradation of methylene blue under UV irradiation," *Journal of Materials Science: Materials in Electronics*, vol. 30, no. 17, pp. 16156–16173, Sep. 2019, doi: 10.1007/s10854-019-01985-8.

[55] M. A. Chougule, S. G. Pawar, P. R. Godse, R. N. Mulik, S. Sen, and V. B. Patil, "Synthesis and Characterization of Polypyrrole (PPy) Thin Films," *Soft Nanoscience Letters*, vol. 01, no. 01, pp. 6–10, 2011, doi: 10.4236/snl.2011.11002.

[56] M. Fabretto, K. Zuber, C. Hall, and P. Murphy, "High Conductivity PEDOT Using Humidity Facilitated Vacuum Vapour Phase Polymerisation," *Macromol Rapid Commun*, vol. 29, no. 16, pp. 1403–1409, Aug. 2008, doi: 10.1002/marc.200800270.

[57] Sheng Hsiung Chang, Chien-Hung Chiang, Feng-Sheng Kao, Chuen-Lin Tien, and Chun-Guey Wu, "Unraveling the Enhanced Electrical Conductivity of PEDOT:PSS Thin Films for ITO-Free Organic Photovoltaics," *IEEE Photonics J*, vol. 6, no. 4, pp. 1–7, Aug. 2014, doi: 10.1109/JPHOT.2014.2331254.

[58] M. Brie, R. Turcu, and A. Mihut, "Stability study of conducting polypyrrole films and polyvinylchloride-polypyrrole composites doped with different counterions," *Mater Chem Phys*, vol. 49, no. 2, pp. 174–178, Jun. 1997, doi: 10.1016/S0254-0584(97)01885-3.

[59] G. Dijk, A. L. Rutz, and G. G. Malliaras, "Stability of PEDOT:PSS-Coated Gold Electrodes in Cell Culture Conditions," *Adv Mater Technol*, vol. 5, no. 3, Mar. 2020, doi: 10.1002/admt.201900662.

[60] C.-L. He, Z.-M. Huang, and X.-J. Han, "Fabrication of drug-loaded electrospun aligned fibrous threads for suture applications," *J Biomed Mater Res A*, vol. 89A, no. 1, pp. 80–95, Apr. 2009, doi: 10.1002/jbm.a.32004.

[61] Y. He, Y. Li, Y. Yuan, J. Shu, X. Deng, and L. Li, "Vapor-Phase Polymerization of PEDOT for Wearable Fabric Pressure Sensors," *J Electron Mater*, vol. 51, no. 3, pp. 1128–1136, Mar. 2022, doi: 10.1007/s11664-021-09388-4.

6 APPENDIX

Appendix A

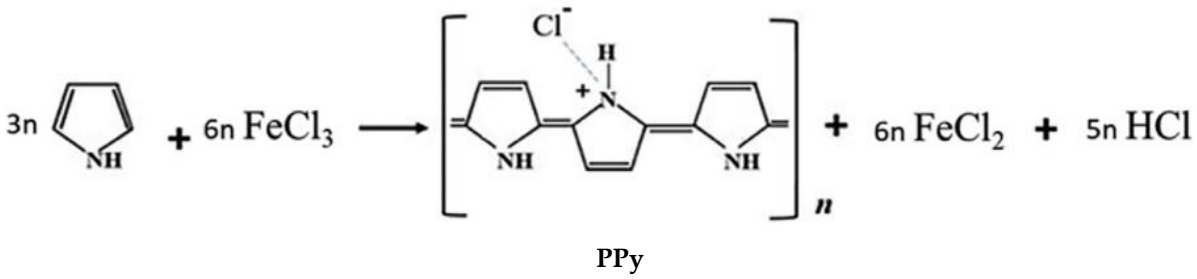

Figure 24: Chemical oxidation of pyrrole. (Adapted from [30]).

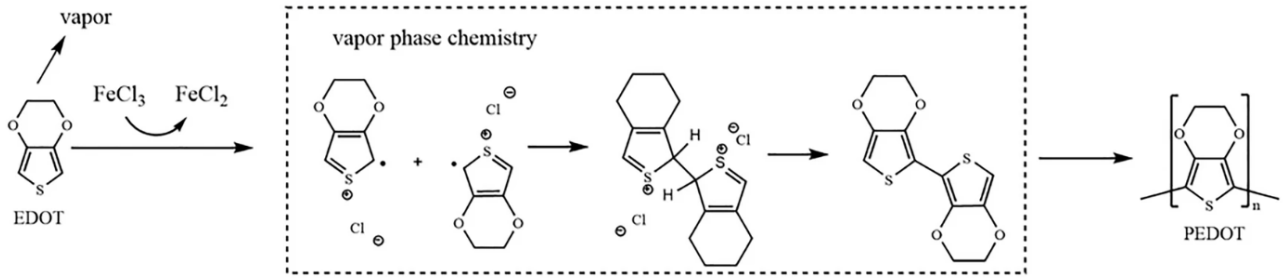

Figure 25: Vapor phase polymerization of EDOT. (Adapted from [61]).

Appendix B

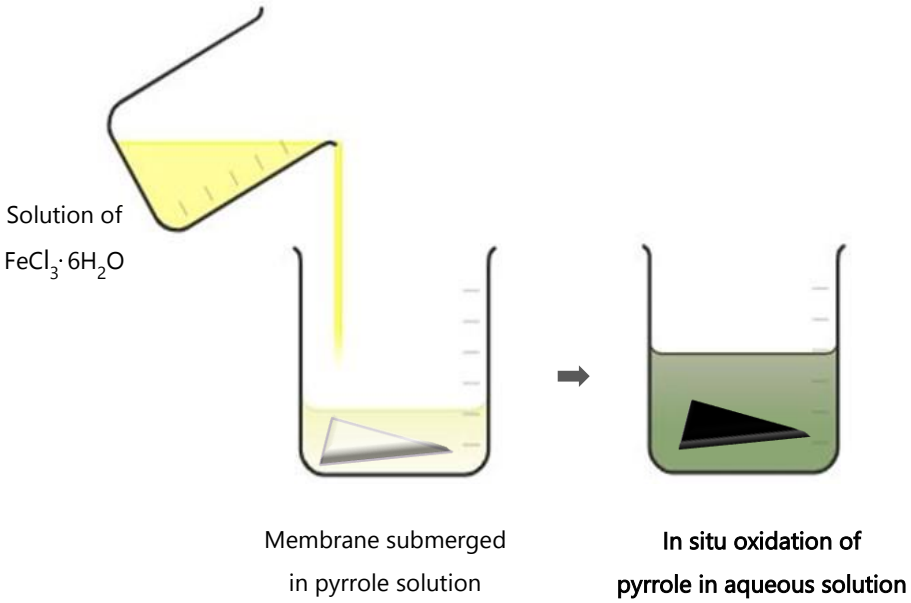

Figure 26: Schematic setup used for liquid phase in situ polymerization of pyrrole.

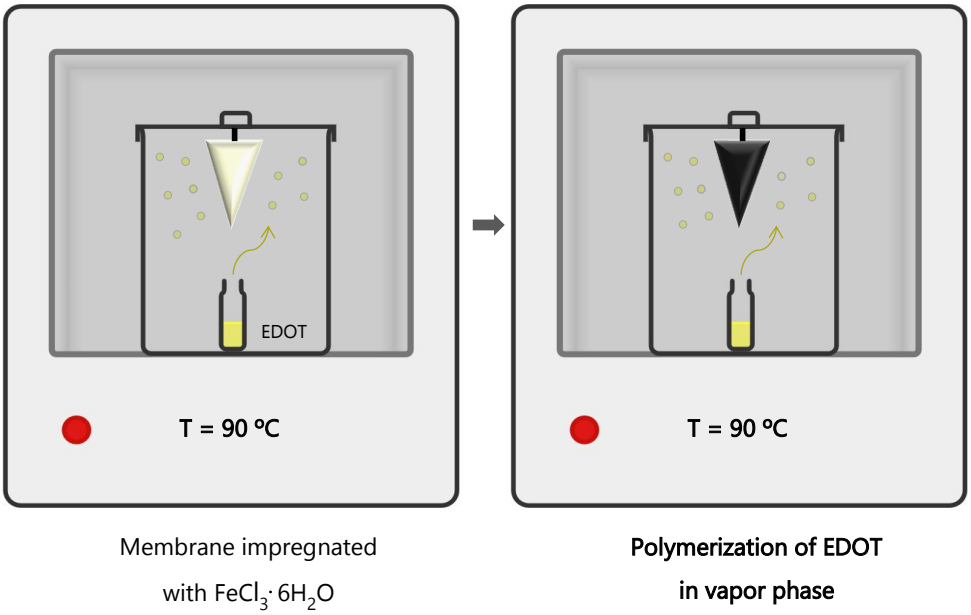

Figure 27: Schematic setup used for vapor phase in situ polymerization of EDOT.

Appendix C

Table 5: Vapor phase polymerization of EDOT in MB:CA membranes.

Parameters	Image	Observations
5h of Electrospinning Polymerization Time = 120min Oven temperature = 90ºC 0.5mL of EDOT	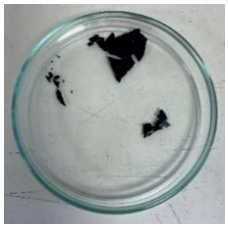	Frangible
8h of Electrospinning Polymerization Time = 120min Oven temperature = 90ºC 0.5mL of EDOT	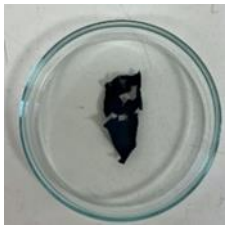	Frangible
5h of Electrospinning **Polymerization Time = 90min** Oven temperature = 90ºC 0.5mL of EDOT	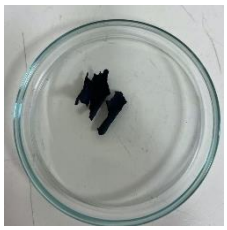	Frangible
5h of Electrospinning Polymerization Time = 120min **Oven temperature = 75ºC** 0.5mL of EDOT	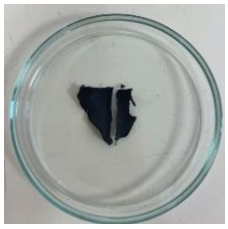	**Less Frangible**
5h of Electrospinning Polymerization Time = 120min **Oven temperature = 75ºC** **0.5mL of EDOT + 1mL of H_2O**	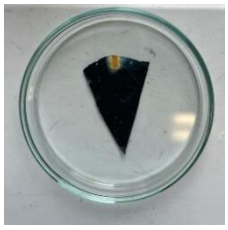	**Non-Frangible**

Appendix D

a.

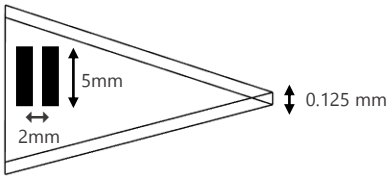

Cross Section Area (A):

= Membrane Thickness x Electrode Length

= 0.125 mm x 5 mm

= 0.625 mm^2

b.

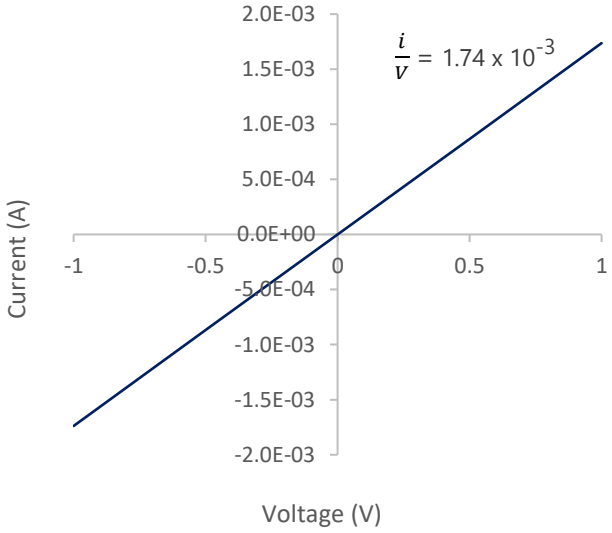

Figure 28: Schematic representation of cross-section area (a) and a model of an I-V curve (b) obtained for the PPy_{90}/MB:CA membrane.

Table 6: Calculations conducted for the measurement of planar conductivity for the PPy_{90}/MB:CA.

Sample	Distance between electrodes = l (mm)	Cross Section Area = A (mm^2)	$\frac{i}{V} = \frac{1}{R}$ (S)	Conductivity = $\frac{l}{A \times R}$	
				Smm^{-1}	Scm^{-1}
PPy_{90}/MB:CA	2	0.625	1.74 x 10^{-3}	5.57 x 10^{-3}	5.57 x 10^{-2}

Appendix E

Table 7: SBF solution components.

Component	Formula	Mass (g)	
Sodium chloride	NaCl	6.547	Sigma-Aldrich
Sodium carbonate	$NaHCO_3$	2.268	PanReacAppliChem
Potassium chloride	KCl	0.373	Scharlau
Sodium phosphate dibasic dihydrate	$Na_2HPO_4.H_2O$	0.178	FLuka Analytical
Magnesium chloride hexahydrate	$MgCl_2.6H_2O$	0.305	PanReacAppliChem
Hydrochloric acid (1M)	1M HCl	15 mL	----------
Calcium chloride dihydrate	$CaCl_2.2H2O$	0.368	Sigma-Aldrich
Sodium sulphate	Na_2SO_4	0.071	Sigma-Aldrich
Tris(hydromethyl) aminomethane	$(CH_2OH)_3CNH_2$	6.057	Sigma-Aldrich
Hydrochloric acid (1M)	1M HCl	"Tritate" up to pH=7.4 at 37ºC	----------

Appendix F

Table 8: Optical Microscopy Characterization of membranes.

CA (100x)	CA w/ PPy (200x)	CA w/ PEDOT (100x)
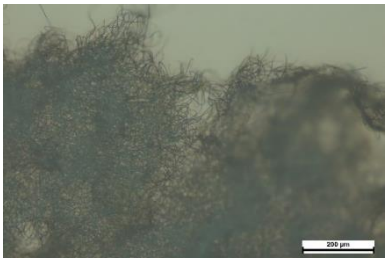	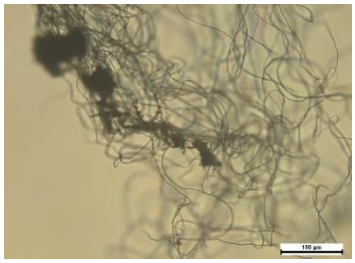	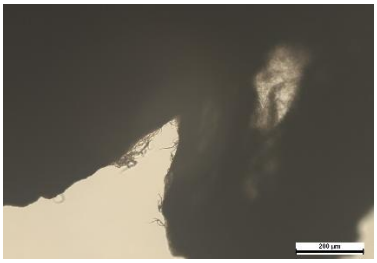
MB:CA (200x)	**MB:CA w/ PPy (100x)**	**MB:CA w/ PEDOT (200x)**
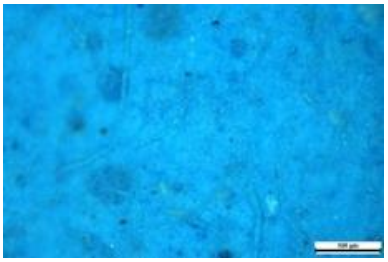	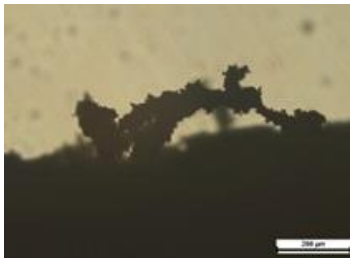	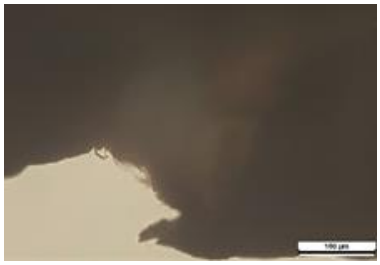

Appendix G

Table 9: Influence of polymerization time in electrical conductivity of functionalized MB:CA membranes.

Samples	Polymerization Time (min)	Membrane Thickness (mm)	Conductivity Average (Scm^{-1})	Standard Deviation (Scm^{-1})
MB:CA	---	0.044 ± 0.006	2.81×10^{-8}	4.69×10^{-9}
PPy/MB:CA	45	0.080 ± 0.013	4.02×10^{-2}	6.99×10^{-5}
PPy/MB:CA	90	0.125 ± 0.034	5.52×10^{-2}	4.01×10^{-4}
PEDOT/MB:CA	45	0.044 ± 0.007	2.93×10^{-1}	8.82×10^{-2}
PEDOT/MB:CA	90	0.040 ± 0.007	6.45×10^{-1}	4.51×10^{-2}
PEDOT/MB:CA	120	0.037 ± 0.006	8.52×10^{-1}	5.68×10^{-2}

Appendix H

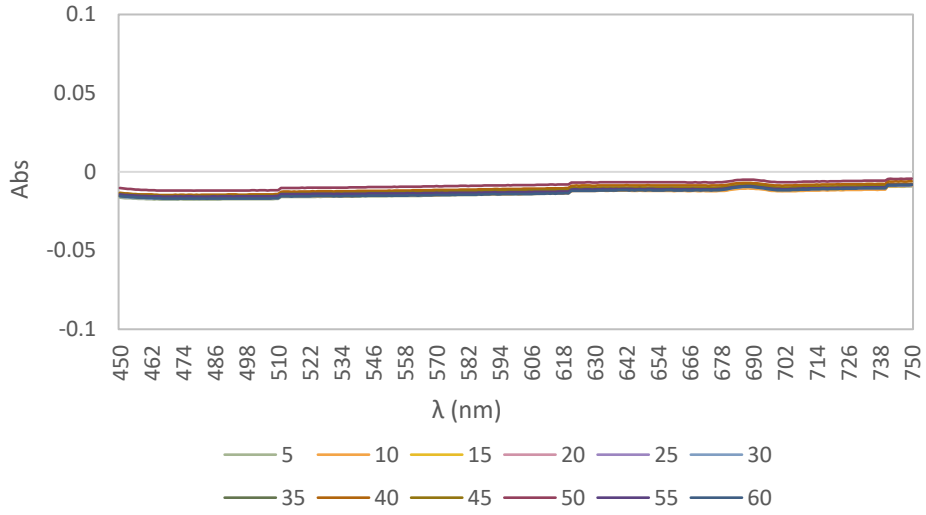

Figure 29: Absorbance spectra of diffusion for the PPy_{45}/MB:CA membrane in SBF.

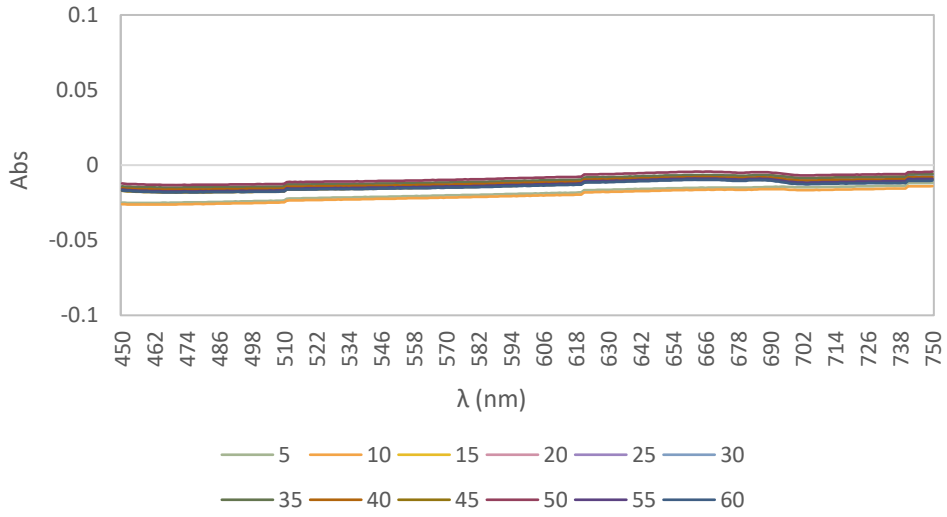

Figure 30: Absorbance spectra of diffusion for the $PEDOT_{120}$/MB:CA membrane in SBF.

Appendix I

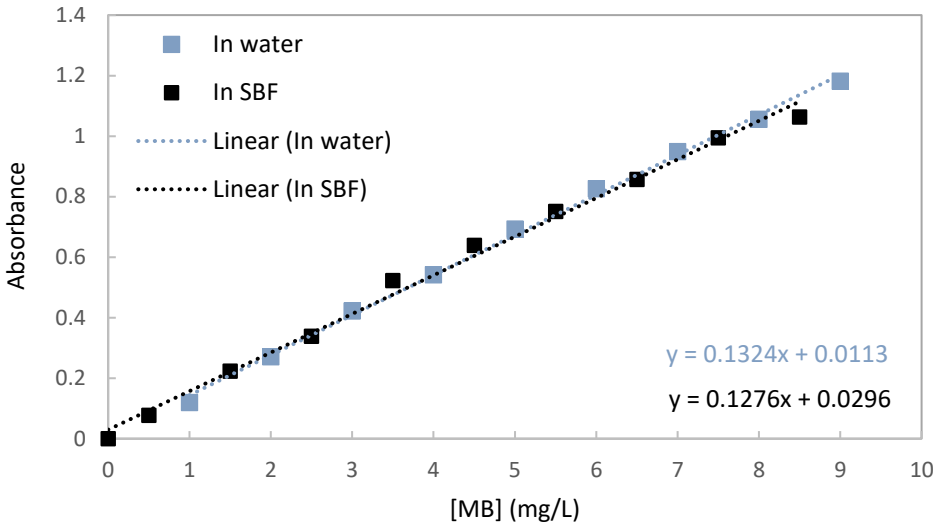

Figure 31: Calibration curve obtained by the maximum absorption value of the peak at 664 nm in SBF and water.

Appendix J

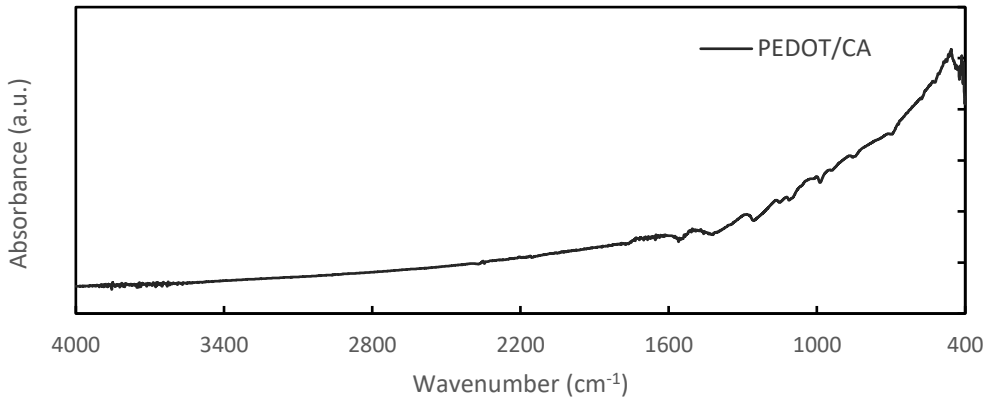

Figure 32: FTIR spectra of PEDOT/CA membrane.

Appendix K

Table 10: Percentage of MB released into SBF according to the respective applied potentials after 1 hour.

System	Potential (V)	Released quantity of MB (µg)	MB (%)
PPy multi-layered system	-0.3	16.3	5
	-0.8	7.68	3
	+0.3	4.60	2
	+0.8	4.00	1
	Diffusion	2.41	1
PEDOT multi-layered system	-0.3	7.83	3
	-0.8	5.29	2
	+0.3	1.49	1
	+0.8	4.68	2
	Diffusion	4.00	1
MB:CA membrane	Diffusion	150	50